

Textile Pressure Sensor: Design, Error Modeling and Evaluation

A dissertation submitted to

ETH ZURICH

for the degree of
Doctor of Sciences

presented by

JAN MEYER

Dipl. El.-Ing. ETH

born 28 March 1978

citizen of Muri b. Bern BE, Switzerland

accepted on the recommendation of

Prof. Dr. Gerhard Tröster, examiner

Prof. Dr. Paul Lukowicz, co-examiner

Acknowledgments

Sincere thanks are due to my advisor, Prof. Dr. Gerhard Tröster, for his support and for providing me with the research facilities and infrastructure at the Electronics Laboratory.

Special thanks belong to Dr. Paul Lukowicz for his willing to act as co-examiner for which I am very grateful and for all his advice during the muscle activity measurement project.

I would like to thank Bernhard Bischoff and Renato Ferrario from Bischoff Textil AG, St. Gallen, Switzerland for their support in manufacturing several prototypes of the sensor textile.

I am grateful to the members of the Electronics Laboratory – past and present – for the pleasant and inspiring atmosphere at the institute. Special mentions go to Tünde Kirstein for her support at the beginning of this thesis and to Bert Arnrich for his help during the posture classification project. I also want to thank Christian Metzger, Friedrich Hanser and Johannes Schumm for their collaboration during different projects.

Finally, I would like to express my gratitude to my parents. Without their support and encouragement this work would not have been possible.

Zurich, October 2008

JAN MEYER

Contents

Abstract	ix
Zusammenfassung	xi
1. Introduction	1
1.1. Pressure sensing in wearable computing	2
1.1.1. Commercial systems	4
1.2. Novel contributions	6
1.3. Overview	6
2. Sensor System	9
2.1. Specification and requirements of the pressure sensor . .	10
2.2. Sensing principle	11
2.3. Design and architecture	12
2.3.1. System overview	12
2.3.2. Architecture of the textile sensor	12
2.3.3. Spacer	20
2.4. Conclusion	21
3. Capacitance Measurement	23
3.1. Requirements	24
3.2. Methods for capacitance measuring	24
3.2.1. Oscillation method	25
3.2.2. Time measurement	30
3.2.3. Charge measurement	30
3.2.4. Current measurement	38
3.3. Parasitic capacitance	38
3.3.1. Two-port method	40
3.3.2. One-Port with active shield	40
3.4. Permittivity of the spacer	42
3.4.1. Compression dependence	42
3.4.2. Temperature dependence	42
3.4.3. Humidity dependence	43
3.5. Comparison and conclusion	45

4. Hysteresis Modeling	47
4.1. Hysteresis phenomena in the textile sensor	48
4.2. Causes for hysteresis	50
4.3. Mathematical models for hysteresis	52
4.3.1. Preisach model	53
4.4. Implementation of the Preisach model	56
4.4.1. Numerical implementation of the Preisach model	56
4.4.2. Declaration of parameter values	58
4.5. Results and conclusion	58
5. Drift Compensation	61
5.1. Drift behavior of the textile pressure sensor	62
5.1.1. Characterization of drift	62
5.1.2. Measurements	63
5.2. Modeling and compensation of drift	65
5.2.1. Implementation	68
5.3. Results and conclusion	70
6. Error Modeling	73
6.1. Introduction	74
6.2. Measurement	74
6.2.1. Experiment setup	74
6.2.2. Experiments	75
6.3. Classification	77
6.3.1. Learning algorithm	77
6.3.2. Features	79
6.4. Error modeling	80
6.4.1. Reference patterns	80
6.4.2. Distance between pressure patterns	81
6.4.3. Noise	83
6.4.4. Hysteresis	83
6.4.5. Drift	85
6.4.6. Sensor failure	85
6.5. Results	85
6.5.1. Classification from modeled patterns	85
6.5.2. Classification from measured patterns	89
6.6. Conclusion	95

7. Conclusion	97
7.1. Summary and achievements	98
7.2. Scalability of the system	99
7.3. Conclusions	99
7.4. Outlook	100
7.4.1. Material and technology	100
7.4.2. Production and commercialization	101
7.4.3. Further use and applications	101
A. APPENDIX A	103
A.1. Error measures	103
A.1.1. Nomenclature	103
A.1.2. Absolute error	103
A.1.3. Relative error	103
A.1.4. Offset	104
A.1.5. Linearity error of AD/DA converters	104
Glossary	105
Bibliography	109
Curriculum Vitae	121

Abstract

This thesis presents a new textile pressure sensor that can be integrated into clothing. The sensing principle of a variable capacitor is used. Electrodes of conductive textiles are arranged on both sides of a compressible spacer. Two basic architectures are evaluated: Perpendicular stripes on both sides of a compressible spacer forming the capacitors at their crossover points and single electrodes on one side and a common electrode on the other side of the spacer. Sensors of various sizes are built with 1, 16, 30 and 240 sensing elements.

The focus of this work is to model the sensor behavior to reduce error sources. By using such algorithms, the field is opened for using standard material and a simple design for the sensor. The models used can be easily adapted to other pressure sensors and even strain sensors.

Errors induced by hysteresis can be reduced from 60% to below 10% by using the Preisach model. Additionally, drift effects are modeled by measuring the step response of the used textile spacer. A new model is developed, reducing drift errors below 5% for a duration of one hour.

Finally, the impact of error sources such as hysteresis, drift, noise and sensor failure is researched for a concrete application: Classification of sitting postures from pressure patterns measured on a seat. The influence of the errors is simulated on the one hand and measured with the classification accuracy and the distance between the classes as measure on the other hand. It is shown that drift effects can be neglected, while modeling the hysteresis enhances the classification rate by 35%. Replacing failing sensors by the mean value of adjacent elements improves the result by 24%. The system with the textile sensor performs similarly to a commercially available pressure mat for this application when the relevant error sources are compensated.

Furthermore, the sensor has shown its usefulness by measuring muscle activity and by supervising the pressure distribution in compression stockings.

Zusammenfassung

Diese Arbeit präsentiert einen neuartigen textilen Drucksensor zur Integration in Kleidung. Er basiert auf dem Prinzip eines variablen Kondensators. Auf beiden Seiten eines reversiblen komprimierbaren Abstandhalters sind die Elektroden aus leitfähigem Textil angebracht, die den Kondensator bilden. Zwei grundsätzliche Architekturen wurden untersucht: Einerseits Sensoren bei denen die Kapazitäten durch parallele Streifen auf beiden Seiten des Abstandhalters angebracht sind. Andererseits wurden Sensoren getestet, bestehend aus einzelnen Elektroden auf der einen Seite und einer gemeinsamen Elektrode auf der anderen Seite des Abstandhalters. Sensoren unterschiedlicher Grösse und mit 1, 16, 30 und 240 Sensorelementen wurden gebaut.

Der Fokus dieser Arbeit richtet sich auf die Modellierung des Sensorverhaltens, um Fehlereinflüsse zu minimieren. Dadurch können Materialien verwendet werden, die nicht speziell für den Einsatz in einem Sensor entwickelt sind. Das Design des Sensors kann vereinfacht werden. Die entwickelten Modelle können einfach für andere Drucksensoren adaptiert werden und sogar für Dehnungssensoren Anwendung finden.

Durch Hysterese bewirkte Messfehler können von 60% auf unter 10% durch die Hysteresemodellierung mittels des Preisach Modells reduziert werden. Zusätzlich werden Drift-Effekte durch die Messung der Schrittantwort des benutzten textilen Abstandsgewirkes modelliert. Durch das neu entworfene Driftmodell kann der Messfehler des Sensors bis unter 5% reduziert werden während einer Messdauer von einer Stunde.

Schliesslich werden die Einflüsse von Drift, Hysterese, Rauschen und Sensorausfällen anhand einer konkreten Anwendung untersucht: Der Klassifizierung von Sitzposturen anhand von Druckabbildern auf einem Sitz. Der Einfluss dieser Grössen wird einerseits simuliert und andererseits anhand der Klassifizierungsergebnisse gemessen. Es wird gezeigt, dass Drift-Effekte einen vernachlässigbaren Einfluss aufweisen während die Modellierung der Hysterese die Erkennungsrate um 35% verbessert. Das Ersetzen von fehlerhaften Sensorwerten durch jeweils den Mittelwert der 4 umgebenden Sensorelemente erhöht die Erkennungsrate um 24%. Durch die Kompensation dieser Einflüsse liegt die Erkennungsrate in vergleichbarem Bereich wie sie mit einer kommerziell erhältlichen Druckmatte erreicht werden kann.

Der Sensor hat zusätzlich seine Brauchbarkeit erwiesen für die Messung von Muskelaktivität zur Bewegungserkennung. Er wurde ebenfalls eingesetzt zur Überwachung des Drucks, der durch medizinische Stützstrümpfe auf das Bein ausgeübt wird.

1

Introduction

Wearable computing, as we know it today, wouldn't be possible without sensors. This thesis discusses pressure sensors. Pressure sensing can give information about activity, movement and even context of the user. The introduction gives an overview of pressure sensors currently used in wearable computing and the open research fields. Subsequently the research focus and an overview of this thesis are given.

1.1. Pressure sensing in wearable computing

Wearable computers play a more and more important role in daily life. In the medical field, personal assistants record all the time the physical data of the wearer [16]. Projects to detect and supervise the physical state in real time are running. Personal assistants guide a worker during the operation and maintenance of machines or building cars [70, 100, 102], protect fire fighters from dangerous situations [53] or help people with back problems [69].

Such devices rely on sensors distributed on the human body. Integrating such sensors directly into clothing has several advantages. Clothing is worn almost anytime and an ideal substrate for mounting sensors. They are just at the right place on the body once dressed and the user doesn't need to care about positioning them. To achieve best integration, textile solutions are favorable. Textile solutions can be made comfortable and unobtrusive for the wearer.

Textiles have been used for pressure [94], stretch [68] and temperature [60, 61] sensing.

Pressure sensing covers a wide field in wearable computing. The activity of different muscles has been measured with force sensitive foil sensors [11, 62]. Sensing muscle activity can help sportsmen train specific muscles or give feedback about the performance quality of exercises for rehabilitation. The activity of the upper arm can be measured by placing a sensor on the biceps and triceps and for the upper legs on the hamstring and quadriceps, respectively. The stiff foil sensors generated problems by fixing them on the skin so that they won't slip away. They are inconvenient for the wearer, too. A textile sensor would be an improvement, since it could be built into underwear with the familiar comfort.

Other force sensitive foil sensors have been developed for robotic applications and artificial skin [12, 50, 63, 96]. MEMS sensors are also used for this application [20, 49, 106]. Artificial haircells measure the flow of air or liquids but could also be used for pressure sensing [19]. A flexible tactile sensing skin based on polymer substrates has been developed in [31]. Such sensors are sufficiently small for unobtrusive integration into clothing. Further research would be needed to get robust attachment onto textiles. An artificial human dermis for pressure measuring can be found in [22].

Upper arm positions have been measured with resistance changing foams [27, 28]. Hysteresis caused by the foam prevents the measurement

of the exact arm positions and only four positions are differentiated. Modeling the characteristics of the foam, specially the hysteresis, would improve this system and make a distinct identification of the arm position possible.

An interest has also been manifested for a body pressure measuring system in the field of prevention of pressure ulcers (decubitus). In the US, 1.3 to 3 million people suffer from decubitus [64, 65]. Medical costs of decubitus in the US vary from US\$ 20.000 to 70.000 per wound [25], and up to US\$ 200'000 per patient for the whole treatment with associated complications [9]. The incidence of pressure sore is 5-10% for hospitalized patients [15, 82], 13% in nursing homes [18], and up to 39% for patients with a spinal injury [9, 55, 114]. There is a high interest in reducing the risk of getting a decubitus. When tissues are exposed to pressure greater than 32 mmHg [58] for prolonged periods of time (5-20 min) blood flow is obstructed and decubitus can occur. Healthy people would feel pain if this limit is reached. For people with disordered sense or those that can't react themselves, a system would be helpful that measures the pressure distribution over time on endangered parts of the body. An alarm for the patient or the medical staff can alert them to turn the body. Alternatively the system could be used for driving adaptive mattresses that change their surface dynamically. The pressure sensing mats for wheelchairs used today are about 10'000 SFr. and more to purchase. This price prevents permanent use and only short time measurements in clinical environment are performed, e.g. for instructing wheelchair users in safe sitting behavior. Textile sensors could be implemented as cushions for wheelchairs, as mattresses for beds or directly integrated into underwear. First prototypes are developed [14, 86] with low spatial resolution (one sensor 10 x 10 cm). Parasitic capacitances are not considered and sensor non-idealities such as hysteresis and drift not compensated.

Commercially available sensor mats have been used to detect the sitting posture in a chair [97, 98, 107]. One sensing mat covers the back and one the seat surface. These provide a resolution of 1x1 cm with 42 x 48 sensing elements each. 127 pressure distribution maps are recorded each second. The pressure images taken are treated like faces and the postures are estimated with distance from future space algorithm. With this system, real time posture detection is possible with a recognition rate of 90 to 99% depending of the postures and 96% in average. In [76] the sensor amount has been reduced to 19 discrete force sensitive foil sensors reaching a classification accuracy of still 78%. The impact

of the quality of the sensor system has not been considered further. There has been no research with regard to effects of non idealities of the sensors such as drift and hysteresis. Sitting postures are also interesting to identify a driver in a car [88], evaluating his behavior [87], or for supervising a passenger in an airplane [7].

In [42] a system is presented to measure sleeping postures by 210 pressure sensors distributed in a bed.

Textile pressure sensors can also be used in intelligent carpets for analyzing dance movements [99], alarm systems or people tracking. Another possible field of application is the supervision of pressure induced by medical stockings on the skin.

1.1.1.1. Commercial systems

Several commercial systems for measuring pressure distribution on the human body are available on the market. *Novel* offers pressure sensitive mats for wheelchairs, horse and bike saddles, insoles and much more. *Tekscan* manufactures pressure sensitive mats for chairs, beds or insoles in different sizes, resolution and pressure ranges. The sensors based on a resistive ink technology, are individually mounted on a flexprint covered by a foil. Also *Medilogic* offers foot measurement systems as insoles and plates mainly designed for walking analysis. The solutions from *Xsensor* are comparable to those from *Tekscan* but use capacitive sensors. The capacitors are formed at the cross-over points of perpendicular conductive stripes on both sides of a compressible spacer. Flexible sitting mats from *GP SoftMess* are based on individual resistive force sensors mounted on a foil carrier. *Trimedico* offers a mat for analyzing pressure distribution in beds.

An overview of selected products can be found in Table 1.1

Implementation into textiles would need modifications of the systems or remains not possible without affecting wearing comfort. They are missing textile properties, e.g. they are not breathable, poorly drapable and can't be washed in a washing machine. Their complexity is also a reason for the high prices.

Hysteresis for the different mentioned products are measured in the range of 19% and drift between 4% and 20% [33, 34].

Products for direct integration into clothing are offered by *Softswitch*. These measure pressure by a composite material that reduces its resistance when compressed [81].

Table 1.1. Selection of commercial pressure sensing systems (2008)

Product	#Sensor elements	Sensor Size	Sampling rate	Accuracy	Pressure range	URL
			sensors			
			mat			
Novel, Pliance	256 (1024)	2x2 cm	20 kHz	5%	0.1-6 N/cm^2	www.novel.de
Tekscan	1024 up to 16'128	1x1 cm	20 kHz (1024 sensors)	10%	0-3.3 N/cm^2	www.tekscan.com
PPS Inc, Tac-Array		2, 2.5, 2.8 mm			0-1400 kPa	pressureprofile.com/ tactArray.php
XSENSOR	up to 65536	1.15-31 mm	up to 40 Hz	16 bit res.	0-200 mmHg	www.xsensor.com/
GeBioM GmbH, GP SoftMess	128-4096	2.4-2.8 cm	30 Hz	5%		gebiom.com
Medilogic	up to 4096	0.75x0.75 cm	82 kHz		0.6-64 N/cm^2	www.medilogic.com/
Trimedico	~4'500	2x2 cm	4.5 kHz			www.trimedico.de/

1.2. Novel contributions

The goal of this work is to design a textile pressure sensor that can be used as an autonomous device or as part of clothing. To improve the sensing quality no special care is taken with material selection. Errors are reduced by modeling the behavior of the sensor.

We want to:

- **design a pressure sensor** that consists of only standard textile materials which is also integrable into clothing or directly part of the clothing and can be treated like clothing (e.g. washable)
- **improve the sensing quality** by modeling the sensor characteristics for reducing effects of hysteresis and drift on the measurement signal
- **find a suitable method to measure the capacitance** of the sensors considering effects such as parasitic capacitances and research the effect of temperature and humidity on the capacitance
- **investigate the influence of errors** such as hysteresis, drift, noise and sensor failures on a concrete wearable application (sitting posture classification) to answer the question how good the quality of such a sensor has to be.

1.3. Overview

In this work we present the design, modeling and evaluation of a textile pressure sensor. Our sensor is based on a capacitive measurement principle and is made from standard textile materials that are widely available on the market. Well known production methods are used. The possibility of direct integration into clothing or ideally, the clothing itself being the sensor has first priority, while increasing the accuracy of the sensor itself has second priority.

This thesis explains the issues and problems of measuring capacitance accurately, modeling hysteresis and drift in the sensor signal and the design of the pressure sensor and its evaluation in a concrete application.

The chapters are structured as follows:

Chapter 2 explains the specification and requirements of the sensor system and describes its architecture and the materials used.

Chapter 3 evaluates different methods to measure the capacitance of the sensor elements.

Chapter 4 focuses on the modeling of the hysteresis caused by the compressible spacer in the sensor to get an accurate pressure value out of the measured capacitance.

Chapter 5 describes the drift behavior of the sensor and how it can be modeled.

Chapter 6 shows the usability of the sensor by investigating the effects of measurement errors such as hysteresis, drift, noise and failure of certain elements in the classification of sitting postures by pressure patterns.

Chapter 7 concludes the work by showing some alternative possibilities and future trends which might drive the integration even further and closer to a future commercial product.

2

Sensor System

This chapter describes the architecture and different designs of the capacitive textile pressure sensor and its materials. Further, specifications and requirements are provided.

2.1. Specification and requirements of the pressure sensor

The task of the pressure sensor is to measure pressure at certain points on the human body over a longer period of time (hours to days). Such a sensor should be unobtrusive and comfortable for the wearer, that means lightweight, soft and flexible. To measure the pressure accurately, it is recommended to place the sensor with direct contact to the skin without any other material (e.g. clothing) in-between to prevent the pressure can be smeared. Unobtrusiveness doesn't only mean that it is not noticeable, but also simple and fast to attach. The sensor should also be insensitive to wrong placing or else wrong placing shouldn't be possible. This can be solved by integrating the sensor into daily clothing. Such integration demands the sensor to survive the washing machine so that it doesn't cause hygienic problems.

A textile solution can fulfill these criteria. Integration into clothing can be more easily compared to mounting bulky or stiff sensors. Parts of the clothing can be used for the sensor, e.g. as carrier for the electrodes. Attaching the sensor onto the textile is possible with textile manufacturing techniques. Robustness is another criteria. The sensor should work after days of wearing and washing multiple times. Textiles normally fulfill this criteria, they are designed for this purpose. On the other hand, conductive textiles can loose their conductivity due to abrasive processes or breaks can occur. The resistance between the connection to the electronics and the electrodes should not exceed 5 k Ω due to the used measurement principle. The change in resistance during the lifetime of the sensor must be low enough so that the 5 k Ω are not exceeded. The conductive material should not lead to shortcuts between parts with different potential. The material or the design of the sensor has to be chosen with respect to this criteria. Furthermore sensor materials shouldn't affect irritations of the skin; e.g. nickel, cobalt or gold can elicit hypersensitivity. Such materials must be avoided.

Pressure range, resolution and size are defined by the application for which the sensor is designed. The sensor presented in this thesis is designed for measuring pressure on the human body. The addressed applications are pressure measuring by sitting in a chair, supervising pressure in compression stockings and muscle activity measurements for arm and leg movement analysis [75]. Pressure induced by sitting has been measured as up to 3 N/cm² in the region of the pelvic bone. For muscle activity it varies from 0 to around 1 N/cm² and up to

0.7 N/cm^2 for compression stockings in the highest class IV [5]. The sensor should be sensitive in a range of 0 to 5 N/cm^2 . To address also other fields of application, the sensor should be easily adaptable for the desired pressure range. The relative error e_r (Appendix A) of commercial solutions for pressure measuring in chairs is around 5-10% (Table 1.1). The textile sensor should also reach this range. The size of the sensor elements depends on the needed geometrical resolution. This is defined by the smallest objects that have to be resolved. The smallest objects are in the size of about 2 cm (e.g. pelvic bone), therefore the spacial resolution of the sensor also should be in this range. Smaller sizes of the sensor elements would increase the amount of sensor elements for covering a given area. This would lead to more complex electronics or to longer measurement time for the whole sensor array when sequential measurement is performed.

2.2. Sensing principle

Several technologies, summarized in [12], have been developed to manufacture plain pressure sensors.

The principle of change in piezoelectric resonance frequency with the applied pressure has been described in [56].

Pressure sensors based on resistive sensors use compressive materials that change their electrical resistance according to the pressure induced. This principle is widely used since measurement is faster than with capacitive sensors and also less susceptible to interference. Force sensitive foil sensors have been used to measure muscle activity [11, 62]. These foil sensors have a certain stiffness and do not breathe and could therefore affect the comfort of the wearer negatively. Pressure sensors with resistance changing foams have been used for coarse sensing of upper arm positions [28]. Four different arm positions with four sensors have been distinguished in [28]. To achieve high accuracy, special care has to be taken when manufacturing the resistance changing materials. Random spatial arrangements of conductive particles in such materials reduce the accuracy [116].

Special care has to be taken to measure the resistance accurately in resistive sensor systems. Resistance of the wires connecting the sensor elements can affect the measurement, mainly when their resistance is not constant. Using the four-wire-method [6] the resistance of the wires is eliminated from the measurement but doubles the amount of wires. The commercially available pressure maps from *Tekscan* use a

resistance changing ink technology. The discrete sensor elements are placed on a carrier foil to form an array. A relative error e_r below 10% is reached with this technology.

Capacitive sensors work on the principle of a variable plate capacitor that changes its capacitance according to the distance of the plates. This distance is dependent on the pressure induced by putting a reversible compressible material in-between. Measurement of capacitance down to aF range is possible with methods known today [110]. Parasitic capacitances can have an impact on the measurement. They can be minimized by an optimal placing and shielding of the electrodes and wires. Measuring methods exist that are insensitive to parasitic capacitances (see later in chapter 3). Shielding is also needed to reduce external effects, such as changing dielectrics on the outside and coupling (e.g. by parts of the body) or to reduce interference with electromagnetic fields (the latter one has also to be investigated for all other types of sensors).

Due to the design possibilities with textile components, due to the available material and good achievable accuracy, a capacitive sensor type has been used in this work.

2.3. Design and architecture

2.3.1. System overview

The pressure measurement system consists of two separate parts (fig 2.1): The textile sensor (array) and the measurement electronics. The sensor can contain one or more sensing elements. Electrical signals were routed by textile wires on the sensor textile to its border where the measurement electronics are connected. In the prototypes, the data is transferred to a PC, but local storage of the measured data in the electronics could be possible.

In the following section, the basic architecture of the sensor array, the connections and the components such as yarn and spacer and the electronics are discussed.

2.3.2. Architecture of the textile sensor

The textile sensor consists of a basic three-layer structure, forming a variable capacitor. The capacitance C of a parallel-plate capacitor of area A is inverse proportional to the distance d between the plates (electrodes) at a given permittivity ϵ of the material between the plates.

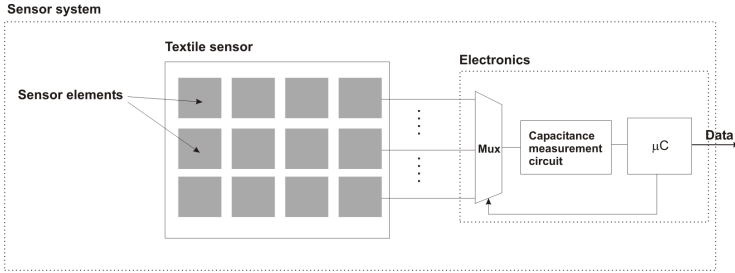


Figure 2.1. Overview of the sensor system.

$$C = \epsilon \frac{A}{d} \quad (2.1)$$

The plates of the designed capacitive sensor are made of conductive textiles. Between these plates, a compressible spacer is arranged that varies its thickness dependent on the pressure induced.

Two main architectures of sensor arrays have been tested: Capacitors formed at the cross-over points of perpendicular stripes and arrays of single electrodes.

2.3.2.1. Stripe electrodes

Stripes of conductive textile that run in parallel across a compressible spacer with perpendicular direction on opposite sides of the spacer form the capacitors at their cross-over points (fig. 2.2). The conductive stripes are woven with conductive yarn in weft direction. The stripes with a width of 2 cm are separated 2 mm by non conductive yarn to ensure proper isolation between neighboring stripes. Pure copper and silver coated copper wires of 40 μm thickness have been used as conductive filament. The filaments have a resistance of 12 Ω/m , resulting in a resistance of one stripe below 1 Ω/m , that fits the specification. The conductive filaments showed themselves to be durable. Since they are fully metal, abrasion doesn't affect the resistance. No breaks and no protrusions have been seen by visual inspection during handling for the studies. No shortcuts between the stripes or reduction of conductivity occurred. Break in a single wire can be bypassed by contacting neighboring wires since non insulated fibres are used.

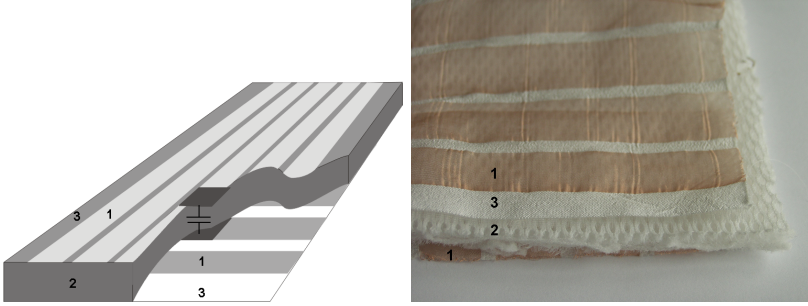


Figure 2.2. Perpendicular stripes of conductive textiles (1) on opposite sides of a compressible spacer (2) form the capacitors at their crossover points. The stripes are separated by non conductive yarn (3)

The stripes not only serve as electrodes but also for signal routing. At the border of the sensor textile, they are connected to cables that are driven to the electronics. The connections to the stripes on both sides of the spacer are switched independently. The amount of connections n_c to the electronics needed is the sum of the number of stripes $n_{s1} + n_{s2}$ on both sides. The number of electrodes n_e formed in the crossover points is the number of stripes of one side n_{s1} multiplied with the number on the other side n_{s2} .

$$n_e = n_{s1}n_{s2} \quad (2.2)$$

Therefore the number of electrodes is larger than the number of connections ($n_e > n_c$) for $n_e > 4$ and $n_{s1}, n_{s2} > 1$. This is a benefit particularly for sensor arrays with a large amount of sensors (> 100) since the number of connections can be kept low. There is a restriction in parallelization of the readout. Parallel measurement within one row or column is possible, but not within separate rows and columns, since multiple crossover points would occur.

The stripe version is limited to rectangular electrodes and uniform sizes when it is fabricated using standard woven techniques. With other manufacturing techniques (embroidering, printing) other forms are possible. The sensing area is not entirely limited to the crossover points, since an electrical field occurs also between the stripes outside this section. This field can falsify the measurement since pressing the neighboring elements changes this field and therefore the capacitance of the

element. This change of capacitance has been measured in the range of 3% when one neighboring electrode is compressed to 50% of unloaded thickness.

2.3.2.2. Array of single electrodes

In the second architecture tested, single electrodes are arranged on one side of the spacer as an array, while the other side consists of one common electrode (fig. 2.3), forming the capacitors between each electrode and the common electrode. Additional layers of conductive textile are arranged covering both sides of the array for shielding purposes.

Electrodes

Prototypes with different numbers of electrodes have been built.

- One prototype is a sensor with one single element (fig. 2.4). Its two electrodes forming one capacitor consist of a woven textile that is coated with silver. The electrodes are sewn on a non conductive textile and arranged on both sides of the spacer.
- An array of separately connected single electrodes forms a sensor that is designed for measuring pressure distribution. Its electrodes on one side of the spacer are embroidered with conductive yarn. The single electrode on the other side consists of the silver coated fabric. Prototypes of 16 (fig. 2.3), 30 and 240 (fig. 2.5) electrodes have been tested.

The size of each electrode is 2 by 2 cm with a distance of 0.7 mm in-between. The grid distance of 2.7 mm is defined by the embroidering process: The needles of the embroidering machines are 2.7 mm in distance. For parallel and therefore fast embroidering, the embroidery pattern has to fit into this grid. The size of 2 cm for the electrodes fits within the specification stated in chapter 2.1.

Connections to the electrodes

Each electrode of the sensor has to be connected separately.

In the prototypes, lines of conductive yarn are embroidered onto the carrying textile to its border where the electronics is connected. For small arrays, less than 5 rows, these lines are routed between the electrodes. A minimal distance d_l of 2 mm between lines and electrodes

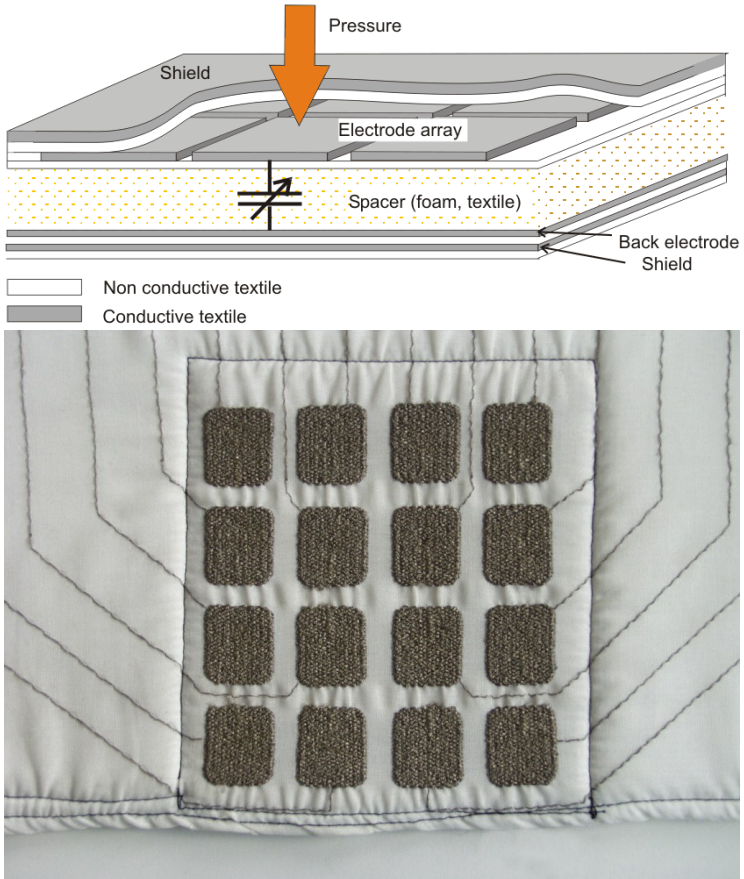


Figure 2.3. An array of electrodes of conductive yarn on one side and a common electrode on the other side of the spacer form the capacitors for pressure sensing (top: Scheme, bottom: Textile prototype with 16 sensing elements, shielding layers removed)

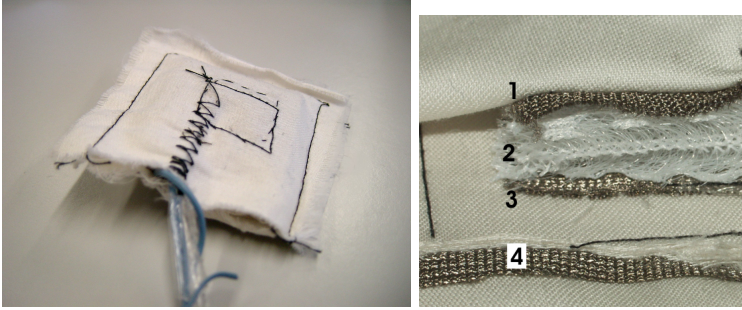


Figure 2.4. Textile sensor with one sensing element. L: Exterior view. R: Cross-section (1: Top electrode, 2: Spacer, 3: Bottom electrode, 4: Shielding layer)

is needed to prevent shortcuts and to keep the parasitic capacitance low. With a spacing d_s of 7 mm, 2 lines can be routed between the electrodes. Generally, the number of lines n_l that can be routed between two electrodes is calculated with

$$n_l = \frac{d_s}{d_l} \quad (2.3)$$

Additional textile layers are used for routing in arrays with more than 5 rows. These layers are separated by layers of non conductive textile to insulate the lines from the electrodes below. For the prototype with 240 elements, three connection layers are needed. In this prototype, the lines are narrowed to the border of the textile to provide a compact connection to the cable to the electronics. The area where the lines are narrowed is coated with silicone to prevent shortcuts. The connection layers are manufactured in three different lengths and for half the width of the array. Each connects 5x8 electrodes, mirrored in the middle of the array (fig. 2.5).

Conductive yarn

Different parts of the sensor that must be electrically connected are sewed together with conductive yarn. Connecting the measuring lines to the electrodes is achieved by sewing the lines over the electrodes. The resistance of these connections has to be below 5 k Ω minus the

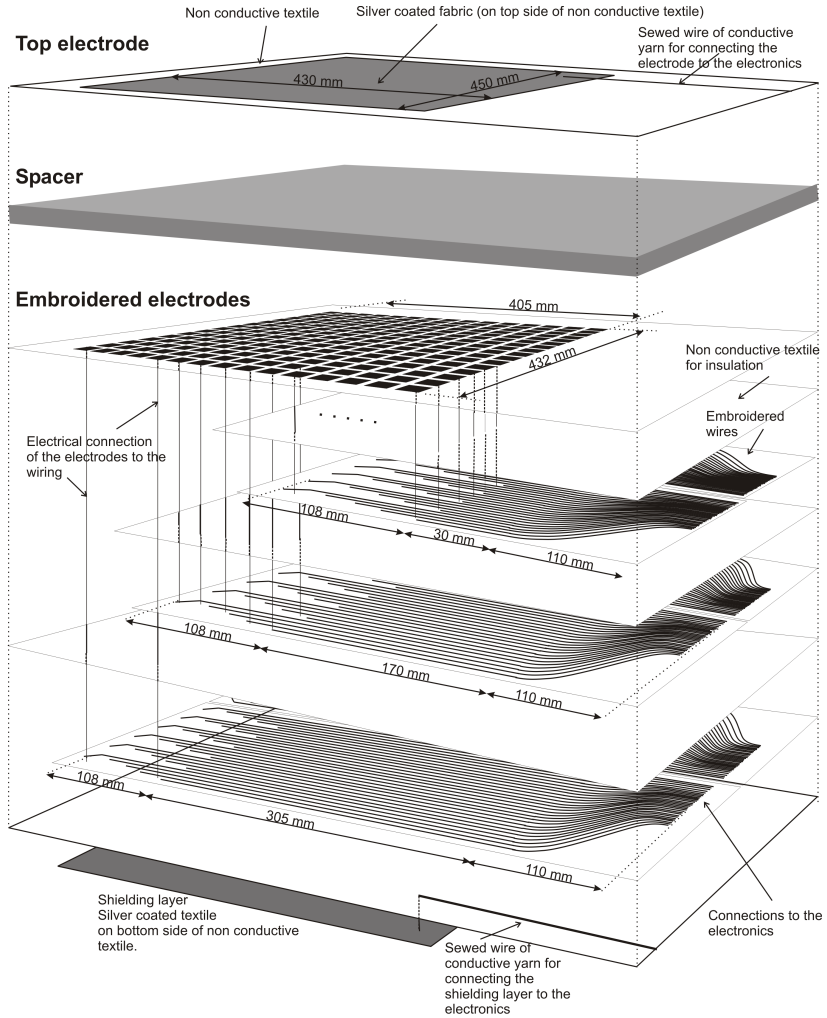


Figure 2.5. Construction of textile sensor with 240 sensor elements. Due to the amount of sensors, three layers are needed for the embroidered connections to the electrodes.

resistance of the lines themselves to achieve the specification. The yarn has to be uncoated at the points of connection and must have a sufficient connecting surface, e.g. the conductive part of the yarn has to be at the outside and not enclosed by the carrier.

Silver coated multi filament polyester yarns and yarns with 2-3 metal fibres that are twinned around a supporting polyester yarn have been investigated for embroidering (fig. 2.6).

The yarn used is a multi filament yarn coated with silver. It is available from *Statex*, type Shieldex 235/34dtx 2ply HC. With a resistance of 120 Ω /m they fulfil both the criteria of low resistance. The resistance increases only a few percent after washing ten times. The filaments of this yarn are twinned together causing a compact yarn. Nevertheless protrusions on the filaments and conductive lint by broken filaments can't be prevented. A single lint of several micrometer thickness can lead to a resistance between two adjacent lines of some hundred Ohm, that already causes a connection between these lines. The number of short-cuts can be reduced through additional silicone coating at vulnerable regions.

The use of insulated yarn could solve the problem with short-cuts. But electrical connection is needed between the yarns within the embroidered electrodes, within the connection lines, so that breaks in the yarn can be bypassed, and between electrodes and corresponding lines. Partial removal of the insulation has been tried but proved itself as not feasible within reasonable effort. Therefore insulated yarn is no option up to now.

Another yarn tested is manufactured by *Philips*. It is the same type of yarn as that from *Statex*, but its filaments are not twinned. This results in a less compact yarn with several times more short-cuts.

Two yarns consisting of metal filaments twinned around a polyester carrier have also been tested. One has three fibres twinned continuously around the supporting yarn in opposite direction and the other consists of two fibres connected together with tangled knots every 1-2 cm. Contacts between the conductive filaments provide an electrical connection between them so that breaks in one filament can be bypassed by another. Both yarns have a low resistance of 7-8 Ω /m. Unfortunately protruding metal fibres formed loops that caused knots and breaks during embroidering what prevents them from further use.

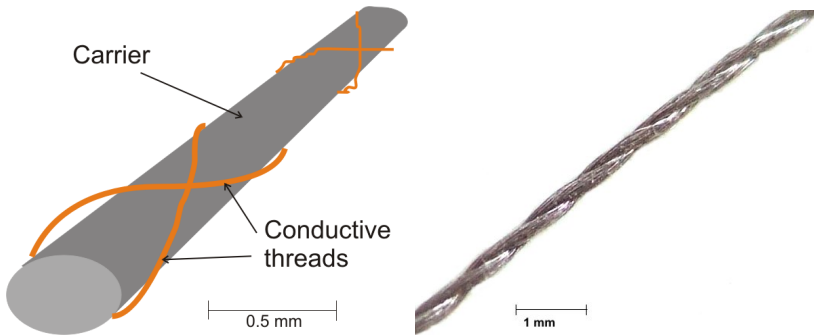


Figure 2.6. The yarns tested for the conductive parts of the textile pressure sensor are polyester yarns with twined metal fibres (l) and silver coated multi filament yarn (r).

2.3.3. Spacer

The spacer between the electrodes defines the pressure range and the resolution of the sensor. The change in thickness at a given pressure is higher in a soft foam than in a more rigid foam. Therefore with a soft foam, small amount of pressure can be measured with higher absolute resolution.

Two different foams and a textile spacer fabric in different thickness have been tested as spacer. The same spacers have been used for both architectures introduced in chapter 2.3.2.

The textile spacer, manufactured by Müller Textil, Germany, is a 3D knit fabric that consists of polyester pile yarns that connect both sides of the spacer, forming a kind of spring (fig. 2.7). We used the product with a thickness of 3 mm and a compressibility of 50% at 1.8 N/cm^2 and one with 6 mm thickness and compressibility of 50% at 2.3 N/cm^2 . A compression-pressure diagram can be seen in fig. 4.1.

The foams used are soft open cell foams. One is a PU foam with a compressibility of 50% at 2.0 N/cm^2 at two different thicknesses of 7 mm and 13 mm and the second one 1.7 N/cm^2 at 50% with 9 mm thickness. The 9 mm foam doesn't recover enough to the initial thickness. After being compressed the thickness is reduced to 8.2-8.4 mm and recovers only after hours to more than 8.9 mm.

The tested spacers are usable to measure pressure in a range of 0 to 10 N/cm^2 . For higher pressure the variation in thickness decreases

since the spacer is compressed to around 70% and further compression needs higher force changes (fig. 4.1). This increases the error above 10%. Therefore other foams would be needed to measure higher forces.

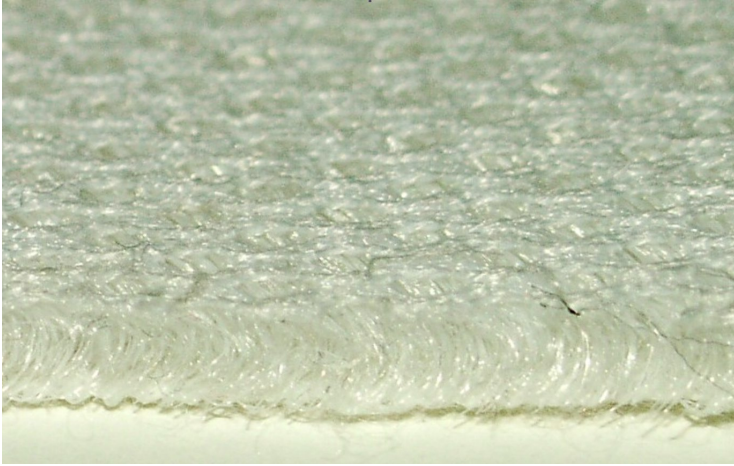


Figure 2.7. Textile Spacer with 6mm thickness and compressibility of 50% at 2.3 N/cm^2

2.4. Conclusion

A design for the textile, capacitive sensor has been found with respect to the requirements for wearability, robustness and sensitivity (section 2.1). Components for such a sensor are available and need no further development. With the chosen design and material the goal of a sensor design employing only textiles can be reached. For smaller sensor arrays (< 100 sensors) the single sensor architecture promises better flexibility in sensor arrangement and higher accuracy compared to the design with perpendicular stripes. This architecture is used for designing the prototypes and further measurements.

3

Capacitance Measurement

In this chapter we will examine capacitance measurement methods that are suitable for measuring the capacitance of the textile sensor elements. These methods must be insensitive to parasitic capacitances that are 20 to 50 times higher than the sensor capacitance. A solution has been found to shield the sensors from electromagnetic interference from the outside and neighbor sensors.

3.1. Requirements

The capacitance of one sensor element has been measured as 2.5 to 8 pF depending on the spacer and pressure for the different prototypes. A wider range of the measurement electronics enhances flexibility in size of the electrodes and selection of spacer. The goal is to keep the relative error e_r of the whole sensor system below 10% (chapter 2.1). The accuracy that has to be reached with the capacitance measurement is set to 1% since other components of the system also induce additional error.

The sensor elements of the sensor array are multiplexed to measure their capacitance (fig. 2.1), so that only one measuring device is necessary. Therefore the measurement technique must be able to measure discontinuously. When parallelization is performed (e.g. to increase the sampling rate), there must be no interference between the different active electrodes and their connections.

For motion detection by measuring muscle activity, sampling rates of at least 10 Hz per sensor element are needed, while update rates of several seconds are enough for sitting applications. 1 to 4 sensors are needed for the muscle application, which leads to a minimal sampling rate of 40 Hz for the system. The number of sensor elements in the cushion sensor for sitting do not exceed 100. A sampling rate of 50 Hz would result in an update rate of two seconds for the whole sensor array, which fits the specification.

No change of capacitance should be measured at the active electrode when pressure changes at adjacent sensor elements. Shielding is needed but that increases the parasitic capacitance between the electrodes, the connections and in the electronics. An appropriate measurement method has to be found so that the parasitic capacitance doesn't increase the error of the capacitance measurement above the desired 1%.

3.2. Methods for capacitance measuring

The capacitance of a capacitor can be measured in different ways. The capacitor can be used as a part of an oscillator and its frequency can be measured. Impedance measurements are another possibility. Charging or discharging a capacitor can also be a measure for its capacitance. The time or current for charging the capacitor or the load on the capacitor can be evaluated. Furthermore there exist some more complex methods

that use a combination of the methods mentioned. An overview over these methods is given in the following section.

3.2.1. Oscillation method

3.2.1.1. Oscillator

The frequency of an RC or LC oscillator depends on the capacitance C_x .

Several implementations of an oscillator are possible. Basic implementation of a RC-oscillator consists of an amplifier ($A(s)$) and a passive RC block ($\beta(s)$) [36, 117] connected in a loop (fig. 3.1). An extension of this model is described in [44, 101]. In most cases OpAmps are used as the amplifier. The amplifier compensates the energy dissipation of the RC/LC block. LC oscillators are similar to RC, but have better phase noise performance [90]. The lowest achievable phase noise PN_{min} of RC relaxation oscillators is [79]

$$PN_{min} \approx \frac{5.9f_0kT}{CV_{src}^2(\Delta f)^2} \quad (3.1)$$

f_0 represents the nominal oscillation frequency, Δf the offset frequency of the circuit, T the temperature, k the Boltzmann constant and V_{src} the supply voltage.

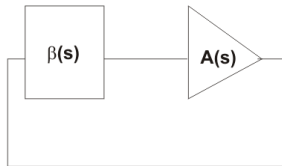


Figure 3.1. Basic oscillator structure.

The frequency of the oscillator is dependent on the implemented circuit, but in all cases it is inverse to the capacitance. For an RC oscillator with given resistance R and capacitance C_x , the angular frequency of oscillation ω_0 is

$$\omega_0 = \frac{K}{R(C_x + C_p)} \quad (3.2)$$

where K is a constant and C_p represents the parasitic capacitance of the system. This parasitic capacitance is also responsible for the baseline drift of the circuit.

The oscillation frequency is measured by a frequency-voltage transducer or a digital counter.

An oscillator is simple to build since it uses only few parts, but it is sensitive to parasitic capacitances. The parallel conductance G_x of the unknown capacitance C_x and the resistance of the wires have an influence on the oscillating frequency. Coupling between the wires at high frequencies can falsify the measurement. Capacitance measurements can be performed in a frequency range of several hundred kHz to a few hundred MHz [43]. The resolution of measurement systems based on RC oscillators is less than 0.01 pF since the frequency is not stable enough; they are not immune to stray capacitances and the frequency is influenced by the shunting conductance of C_x [45].

3.2.1.2. Resonance method

The resonance method is shown in [29] and [110]. An RC or RLC circuit is tuned to resonance and the resonance frequency ω_r is measured. This frequency depends on the capacitance, $C_x = f(\omega_r)$.

An inductance L is added in parallel to the unknown capacitance C_x . The frequency of the source voltage V_{src} is tuned to the resonance frequency of the RLC oscillator. If the circuit is in resonance, the unknown capacitance C_x can be calculated from

$$C_x = \frac{1}{(\omega_r)^2 L} \quad (3.3)$$

The circuit is in resonance when the phase shift between V_{src} and from the current I_r in the LC circuit is zero [108]. The frequency of the source voltage V_{src} can be tuned by a feedback loop I_r to V_{src} . PLLs are used for the feedback loop in [111] and [108]. An implementation of this circuit to measure capacitance changes in fF range with an accuracy of 50 fF can be found in [111].

This circuit can be also implemented with a resistance instead of an inductance (RC resonator).

If the RLC resonator is connected as shown in fig. 3.2, so that one electrode of the capacitance is grounded, the circuit is sensitive to the parasitic capacitance C_p 1:

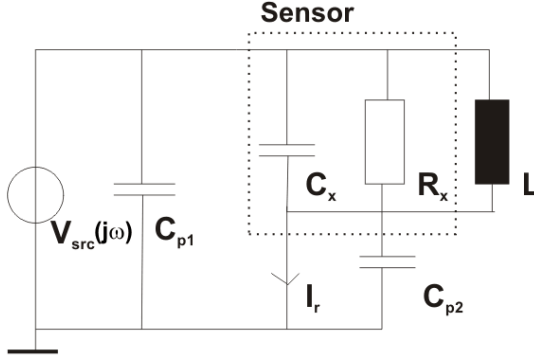


Figure 3.2. Resonance Method.

$$C_x + C_{p1} = \frac{1}{(\omega_r)^2 L} \quad (3.4)$$

The parasitic capacitance C_{p2} doesn't influence the resonance frequency and can be neglected.

Another approach is to connect the impedance in series to the unknown capacitance to build a series RLC circuit. A series resonator using a PLL is shown in [39]. However, the circuit in [39] is based on the assumption, that the capacitance is slowly varying over time, and that can't be guaranteed as a sensor. This resonance circuit can be used with relatively small parallel resistances that means dielectrics with high loss factors. With the double-resonance method developed by [46] dielectrics with a loss resistance of 30Ω can be used.

3.2.1.3. Impedance measurement

An AC Voltage $V_{src}(j\omega)$ with a given frequency f_{src} is connected to the unknown capacitance C_x . The impedance Z_x of the capacitance C_x is measured by measuring the current I_c through the capacitance. A possible implementation of this method uses a series resistor R_s connected to the capacitance. The voltage $V_R(j\omega)$ over this resistor is proportional to the current I_c , so Z_x may be calculated as

$$Z_x = \frac{1}{j\omega C_x} = \left(\frac{V_R(j\omega)}{R_s(V_{src}(j\omega) - V_R(j\omega))} - \frac{1}{R_x} \right)^{-1} \quad (3.5)$$

If the ohmic resistance R_x of the capacitance C_x is high enough ($R_x \gg R_s(V_{src}(j\omega) - V_R(j\omega))/V_R(j\omega)$), R_x can be neglected and eq. 3.6 simplified to:

$$Z_x = \frac{1}{j\omega C_x} = \frac{R_s(V_{src}(j\omega) - V_R(j\omega))}{V_R(j\omega)} \quad (3.6)$$

Another implementation that measures the admittance by using an OpAmp is explained in [29] and shown in fig. 3.3.

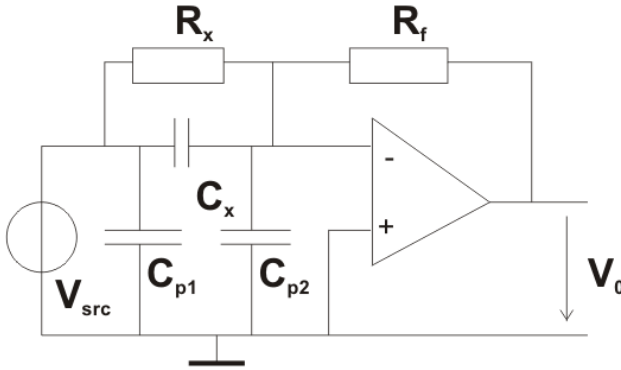


Figure 3.3. Circuit to measure admittance of the unknown capacitance C_x

The output voltage of this circuit is

$$V_0(j\omega) = -(j\omega C_x + 1/R_x)R_f V_{src}(j\omega) \quad (3.7)$$

This implementation is insensitive to the parasitic capacitances C_{p1} and C_{p2} .

The influence of the admittance R_x on the output voltage is reduced at higher frequency as can be seen in eq. 3.7. The authors in [95] used this method in a textile pressure sensor; the influence of switching the capacitances in a sensor array is further explained there. They measured capacitances down to 100 fF.

3.2.1.4. Capacitive bridge

The capacitive bridge is a method for accurate measurement of small capacitances, based on the Wheatstone bridge. It's a special implementation of the impedance measurement method.

The unknown capacitance C_x is compared with known, accurate capacitance C_{ref} and impedances Z_1 and Z_2 forming a voltage divider as shown in fig. 3.4.

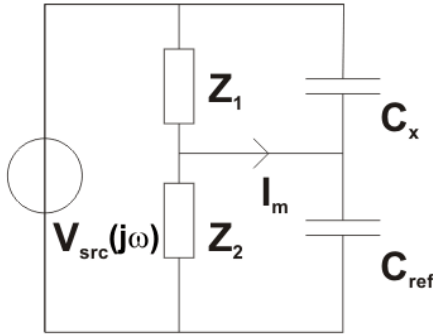


Figure 3.4. Capacitive bridge

The bridge is in balance, if I_m is 0, that means $Z_1/Z_2 = C_{ref}/C_x$. To reach this point, either C_{ref} , the ratio Z_1/Z_2 or both can be tuned. Another possibility to quantify C_x is to measure the current I_m

$$I_m(j\omega) = j\omega V_{src}(j\omega)(C_x - C_{ref}) \quad (3.8)$$

in the bridge with a fixed reference capacitance C_{ref} . V_{src} and ω need to be of a known value.

This method has been implemented in [119] with a resolution of 2.5 fF and noise level of 0.6 pF.

Another variant is to measure the imbalance of the bridge with a voltage meter [45].

3.2.2. Time measurement

3.2.2.1. Time constant measurement

The capacitor is loaded over a resistor with resistance R_L by a voltage source with voltage V_{src} (fig. 3.5). At time τ the capacitor is loaded to

63.2% and the capacitance C_x is

$$C_x = \frac{\tau}{R_L} \quad (3.9)$$

The time τ to load the capacitor limits the maximum sampling rate of measuring the capacitance values since the measurement time for one sample is at least τ .

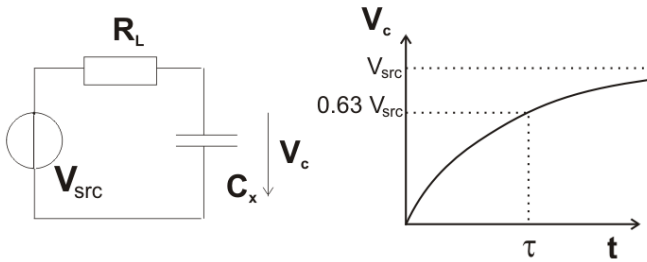


Figure 3.5. Time constant measurement. L.: circuit, r: Voltage V_l over the capacitor while loading with constant current

Another possibility is to load the capacitor during a defined time and to measure the voltage over the capacitor at the end of the loading cycle. This method is easier to implement than the one mentioned above since only a voltage measurement has to be performed. It is similar to the charge-discharge method mentioned in the next section.

3.2.3. Charge measurement

3.2.3.1. Charge-discharge method

The capacitor C_x is charged to the voltage V_{src} and then discharged to a charge amplifier (fig. 3.6) to measure the charge loaded on the capacitor. The average discharging current is

$$I_x = V_{src} f C_x \quad (3.10)$$

while f is the frequency of switching between charging and discharging.

Several design possibilities exist for the charge amplifier, with OpAmps (fig. 3.6) or integrated over a RC low pass filter. Some implementations are shown in [29].

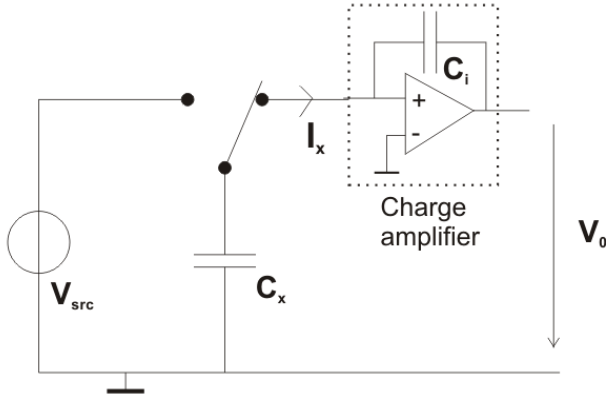


Figure 3.6. Principle of the charge-discharge method

The current into the load detector is transformed with a capacitance C_i in a voltage. C_i is significantly bigger than C_x . The output of the detector is a voltage V_0 proportional to the charge. V_0 depends on the capacitance C_x as follows:

$$V_0 = V_{src} \frac{C_x + C_{p1}}{C_i} \quad (3.11)$$

The noise is reduced if n charge/discharge cycles are applied without discharging C_i . Then the capacitance is calculated as

$$C_x = C_i \frac{V_i}{V_{src}} \frac{1}{n} - C_{p1} \quad (3.12)$$

The method is not stray-immune.

An implementation is shown in [2] for a capacitance range of 2.2 pF to 2.2 mF. The output voltage V_i is proportional to C_x . The measurement time is longer than with the time constant measurement method, since the capacitor has to be fully loaded.

Further details are given in [29, 45, 80]. This method has been patented by Endress and Hauser Ltd [30].

3.2.3.2. Constant charge operation

The constant charge method measures capacitance changes by holding the charge constant on a capacitor when its plates are moving. Two implementations are possible: Charge or voltage driving [77].

Voltage driving

A voltage source V_{src} is connected via a resistor R_{bias} to the capacitor C_x . By moving the capacitor plates sufficiently fast, the charge on the capacitor keeps constant and an ac voltage occurs between the plates, depending of the space x between the plates (fig. 3.7).

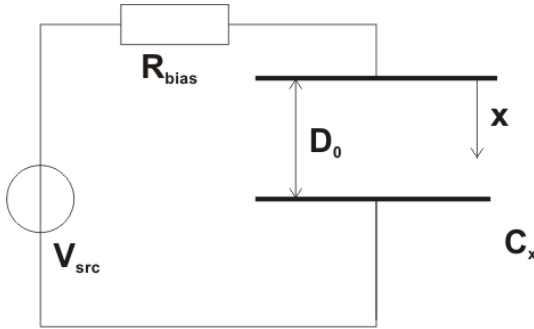


Figure 3.7. Model for operation with constant voltage source

Charge driving

The charge of the capacitor is held constant by two current sources, while the distance of the moving plates is changing. This results in an ac voltage V_o over the capacitor that is inversely proportional to the capacitance:

$$V_o = \frac{Q_o}{C_0 x_0} \frac{\epsilon A}{C_x} \quad (3.13)$$

where Q_o represents the charge and C_0 the capacitance at a given plate distance x_0 .

These methods are commonly used in microphones, rather than in pressure sensors due to the need for high stimulating frequency. Con-

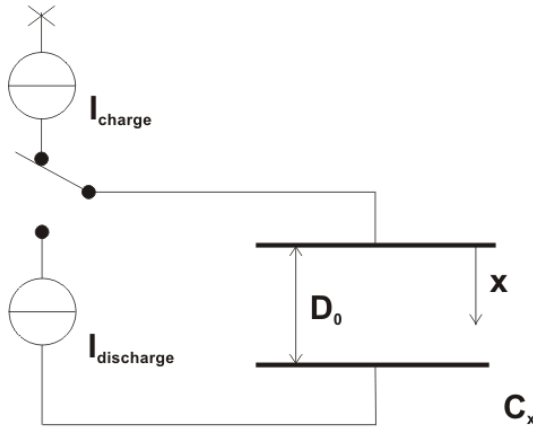


Figure 3.8. Block diagram of the constant charge operation method

stant measurement is needed, since only capacitance changes are measured. Therefore it is not applicable for sequential measurement of a capacitor array or for constant capacitances.

Further details about this method can be found in [78].

3.2.3.3. Smart charge redistribution

This method is an improved version of the charge-discharge method presented by Kung [57]. An implementation is shown in [110] and at fig. 3.9.

The unknown capacitance C_x is measured by comparing the charging voltage with the voltage over a reference capacitance C_{ref} . Charging of the two capacitances is controlled by a microcontroller. In Kung's solution [57] C_x and C_{ref} are switched simultaneously and loaded from ground to a voltage V_{ref} while switch S_1 is closed. Then S_1 is opened, C_x grounded and V_{ref} applied to C_{ref} . The voltage V_{DAC} of the DAC is set to

$$V_{DAC} = V_{ref} \frac{C_x - C_{ref}}{C_f} \quad (3.14)$$

to set the input voltage of the amplifier to 0. This voltage is proportional to the difference between the capacitances C_x and C_{ref} .

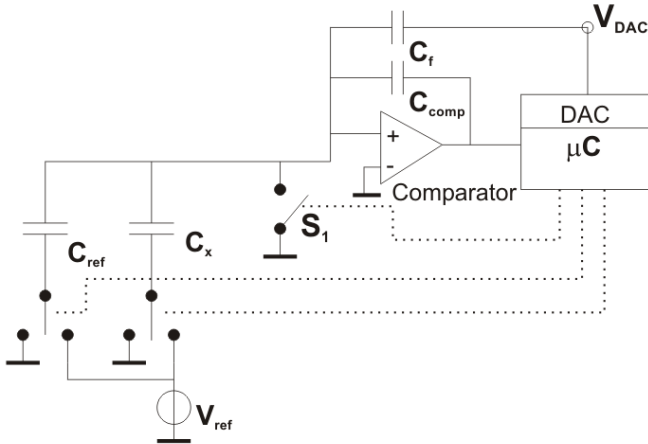


Figure 3.9. Block diagram of the smart charge redistribution method

Toth [110] altered this solution by measuring C_{ref} and C_x separately so as to measure V_{ref} and also C_f .

With a 12 bit D/A converter, 24aF resolution can be achieved in a measurement range of 0 to 100 fF. The measurement time expected by [110] is less than 1 ms, based on the conversion time of 20 μs by Kung [57]. The comparator's gain must be high enough to be insensitive to parasitic capacitances, e.g. for a parasitic capacitance C_{p1} of 100 pF larger than $4 * 10^6$ [110].

3.2.3.4. Modified Martin oscillator

Martin [67] presented a switched capacitor oscillator that was modified by Van Dreht [24]. This modified version is called modified Martin oscillator (fig. 3.10). It's a linear capacitance controlled oscillator. The modified Martin oscillator is similar to the charge-discharge method, but when the capacitor C_x is charged, an opposite charge is simultaneously stored in the charge amplifier. The charge amplifier is built with the capacitance C_1 and the corresponding opamp. The amplifier is discharged by a resistor R. The second opamp acts as comparator to switch between charging and discharging the capacitance C_x . Imperfect shielding between the charge amplifier and the comparator results in

the existence of a capacitance C_{offset} .

The period T of the modified Martin oscillator is [109]

$$T = 4R(C_x + C_{offset}) \quad (3.15)$$

C_{offset} can be measured by removing C_x .

The non-linearity has been found as 0.1 % in a measurement range of 50 fF with a measurement time of 300 ms [109]. For a 2 pF range the error increases to 0.4%.

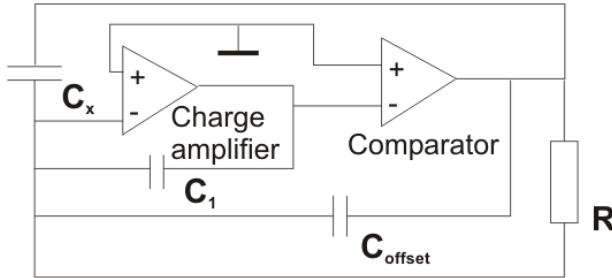


Figure 3.10. Modified Martin oscillator

An improved version is shown at [109]. The resolution is 20 aF with an non-linearity of 100 ppm and a measurement time of 300 ms. Details concerning different error sources are given in [109].

3.2.3.5. Multiple-sensor modulator

The multiple-sensor modulator is originally presented by Van der Goes [112]. A circuit for capacitance measuring can be seen in fig. 3.11.

Resistive and capacitive sensor elements can be measured by this circuit. Capacitance measurements [38] are performed with a charge amplifier whose output voltage is converted to a period, using the charge-discharge method. This signal is used to drive the capacitances, thus forming a capacitance controlled oscillator. A detailed description can be found in [38].

The multiple sensor modulator is implemented into a commercial IC, the Universal Transducer Interface by *Smartec BV* [8]. It can measure capacitances in three ranges from 0 to 2 pF, 0 to 12 pF or up to 300 pF with a measurement time of 5 ms and a resolution of 50 aF

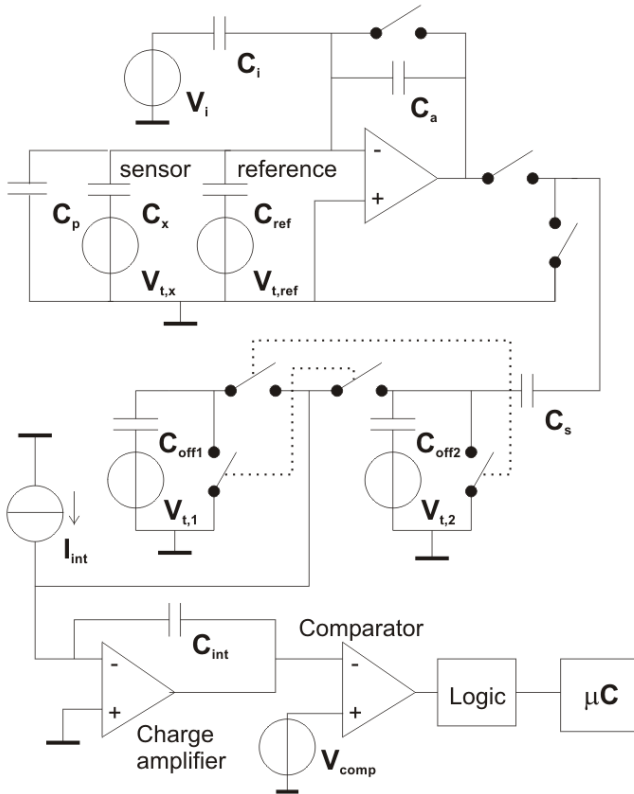


Figure 3.11. Multiple sensor modulator in capacitance measurement mode

[110]. The parasitic capacitance at the input $C_{p1} + C_{p2}$ is allowed to be up to 300 pF. The non-linearity is less than 250 ppm and the offset less than 15 fF [110]. The 3-signal auto-calibration method [72, 113] is applied with a reference capacitor C_{ref} to eliminate the effects of additive and multiplicative errors.

3.2.3.6. Capacitance to digital converter (sigma-delta converter)

Sigma-delta is a well proven technology that has been used for years in high-performance (>18 bits) ADCs. Two constant capacitors, C_{in}

and C_{ref} are periodically switched to the voltage V_{in} that has to be converted, and the reference voltage V_{ref} . They charge an integrator consisting of C_{int} . A comparator using the output of the integrator as input produces the output signal of the sigma-delta converter. Positive value of the integrator leads to output 1, negative value to 0.

This technology can be used for capacitance sensing when the input voltages are fixed instead of the capacitors. One capacitor is replaced by the sensing capacitor and the defined voltage over this capacitor can be understood as an excitation voltage. A block diagram can be seen in fig. 3.12.

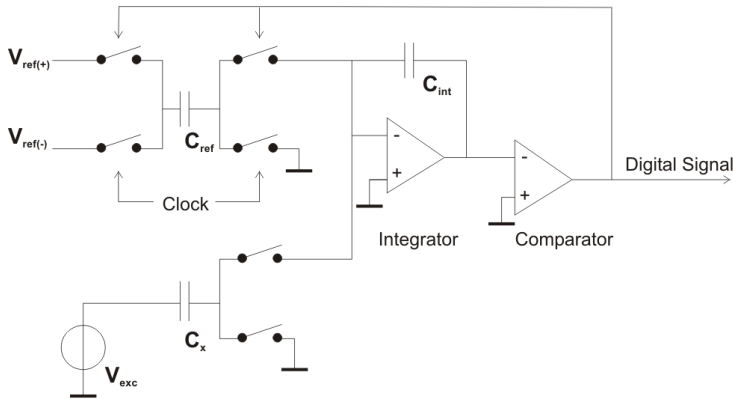


Figure 3.12. Sigma-delta converter for capacitance measuring

The output data of the converter represents the ratio between the sensor capacitance C_x and C_{ref} .

This technology has been implemented in the commercially available ADC from Analog Devices, the AD7745. The AD7745 is a 24-bit sigma delta converter with a measurement range of 8 pF, accuracy of 4 fF and a linearity of 100 ppm at a sampling rate of up to 90 Hz [1]. The device is tolerant to parasitic capacitance to ground up to 60 pF without affecting the measurement. For larger parasitic capacitances the accuracy is decreasing. For parasitic capacitance C_{p1} of 200 pF, the error amounts to 0.5 fF and for $C_{p2} = 200$ pF the error is 5 fF for an operating voltage of 3 V.

3.2.4. Current measurement

3.2.4.1. Constant current operation

The current I_c to load a capacitor is proportional to the derivation of the voltage V over the capacitor:

$$I_c(t) = C \frac{dV}{dt} \quad (3.16)$$

If dV/dt is piecewise constant, e.g. by using a triangular voltage, I_c is also piecewise constant and the absolute value is proportional to C .

A circuit has been implemented in [80] with a resolution of 10 fF.

3.3. Parasitic capacitance

Parasitic capacitances can reduce the measurement quality. In the textile sensor, parasitic capacitances occur in several areas:

- between adjacent electrodes and wires
- between the wires and the common electrode
- in the measurement electronics

The influence of parasitic capacitance can be reduced by using shield electrodes. In the textile sensor, the capacitance of only one sensor element is measured at a time. The other electrodes are used as guard by connecting them together to the guard potential. Since the wires to the electrodes are all in parallel, the active wire is sufficiently shielded by its neighbors. An additional guard electrode is arranged at the outside around the whole sensor array to reduce influences from the outside (fig. 3.13).

The parasitic capacitances from the sensor to the shield are represented by C_{p1} and C_{p2} (fig. 3.14). The shield is usually connected to ground. C_{p1} is the parallel connection of the parasitic capacitances between the active electrode and the neighbor electrodes with their connections and between the active electrode and the shield. C_{p2} represents the parasitic capacitance between the common electrode and its connection to the shield and between the non active electrodes and their connections.

Capacitances between the shield and the active electrode have been measured as 100-150 pF in the cushion version of the sensor (sensor

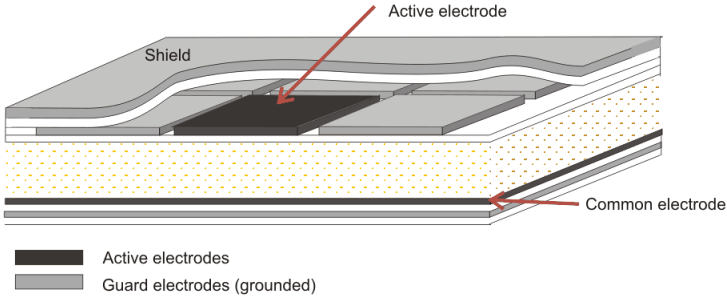


Figure 3.13. Shielding the textile sensor with guard electrodes

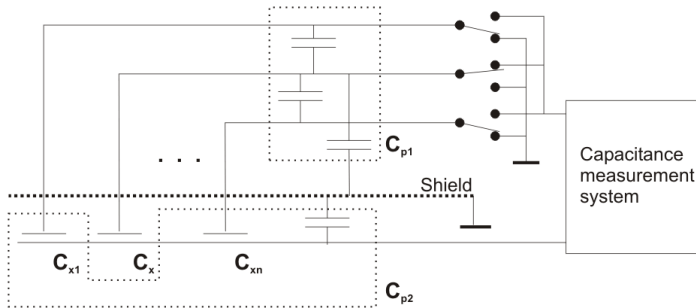


Figure 3.14. Parasitic capacitances of the sensor system.

with 240 elements), depending on the selected electrode. This is significantly higher than the capacitance of a sensor element of about 2.5 - 8 pF. Therefore, a measuring method is needed that is insensitive to parasitic capacitances. Two methods are commonly used, the two-port measurement and the one-port with active shield.

3.3.1. Two-port method

How to deal with the parasitic capacitance with the two-port method is presented in [110]. The influence of C_{p1} and C_{p2} can be reduced by short-circuiting them. This can be achieved by driving the potential of C_{p1} by a voltage source V_{src} with low impedance R_{src} (fig. 3.15). The

impedance has to be low so that charging C_x is not affected by C_{p1} . The relative error e_r of the voltage on C_{p1} after a certain time t is [110]

$$e_r = e^{-t/\tau} \quad (3.17)$$

with the time constant τ

$$\tau = R_{src}C_{p1} \quad (3.18)$$

C_{p2} is connected to a charge or current amplifier. V_{out} depends only on the input voltage and ratio between C_x and C_f if we assume the input resistance, bandwidth and gain of the opamp and the parallel resistances of the parasitic capacitances are infinite

$$V_{out} = -V_{src} \frac{C_x}{C_f} \quad (3.19)$$

In this case the voltage over C_{p2} is zero. For a real opamp with limited bandwidth f_T the error is calculated with eq. 3.17 and time-constant [110]

$$\tau = \frac{C_f}{2\pi C_{p2} f_T} \quad (3.20)$$

Limited gain A of the opamp and input resistance R_{in} lead to an additional error with time constant [110]

$$\tau = C_f R_{in} A \quad (3.21)$$

The two-port method is used for the smart charge redistribution (Chapter 3.2.3.3), impedance measurement (Chapter 3.2.1.3), modified Martin oscillator (Chapter 3.2.3.4), multiple sensor modulator (Chapter 3.2.3.5) and in the AD7745 (Chapter 3.2.3.6).

3.3.2. One-Port with active shield

If one electrode of the measurement capacitor is connected to ground, two-port measurement can't be applied. For this purpose the one-port measurement with active shield is often used. The shield electrode is driven at the same voltage as the active electrode, reducing the potential between them to zero (fig. 3.16). This method does not eliminate the parasitic capacitance of the measuring circuit. It is also difficult to build a suitable precise voltage follower, specially at frequencies above 1 MHz [45]. In [85] an active shield method has been developed that

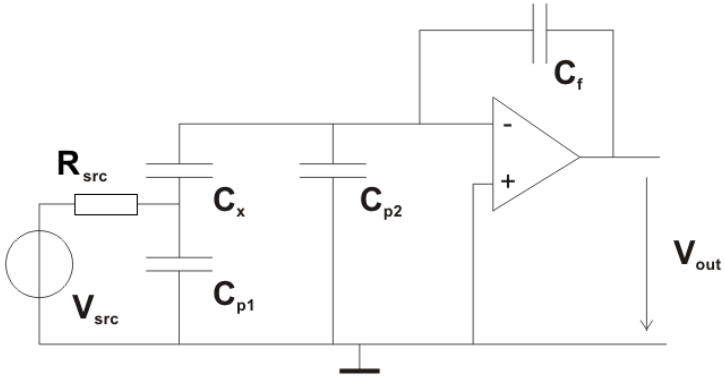


Figure 3.15. Circuit to reduce the parasitic capacitances to ground.

measures capacitances to ground in a range of 27 pF to 330 pF with parasitic capacitances between shield and ground of 1000 pF with a relative error e_r of less than 0.12%.

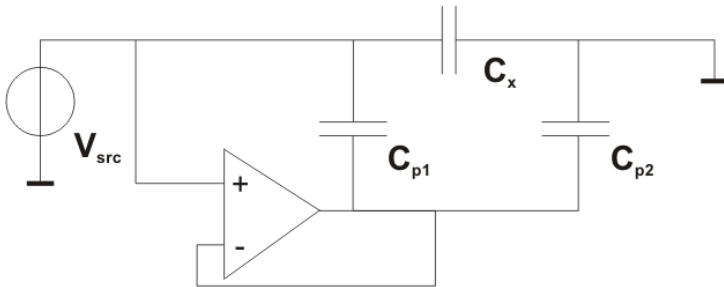


Figure 3.16. One-Port with active guard method

3.4. Permittivity of the spacer

The compressible spacer between the sensor electrodes has an impact on the capacitance measurement by its permittivity. The capacitance changes not only according to the distance of the electrodes by different

compression, but also by a variation of the permittivity of the spacer due to compression. Since a calibration is needed for calculating the pressure out of the capacitance value, variation of the permittivity due to compression is neglectable. In contrast, changes of permittivity over time, not induced by pressure changes, influences the measurement. Such alternations could occur due to aging and changes in the material of the spacer, humidity or temperature.

3.4.1. Compression dependence

The foams and textile spacer employed consist mainly of air in the uncompressed state; the volume-fraction of material is less than 5%. Therefore, their relative permittivity is comparable with air, e.g. for soft PU foam it is in the range of 1.0 to 1.1 [92]. If an open cell foam is completely compressed, that means all air is removed, the permittivity becomes the same as the material of which the spacer consists. In closed cell foams the air can't be removed without irreversibly destroying the cell structure, but it is compressed to a minimal volume. Common foam materials such as polypropylene, polystyrene, polyethylene and polyurethane have permittivities of 2.1 [3], 2.4-2.7, 2.25 [4] and 3.5 [104] respectively at room temperature and 1 kHz. Relative permittivity ϵ_r (to vacuum) of the textile spacer of 6 mm thickness (Chapter 2.3.3) is 1.14 at 2.4 GHz [61]. This has been evaluated by the authors of [61] with S-parameter measurements of two microstrip transmission lines of different lengths as explained in [41]. When the spacer is compressed to 30% ϵ_r increases to 1.6 (fig. 3.17).

3.4.2. Temperature dependence

Permittivity of the textile spacer and the used foams have been measured for temperatures between 10 and 30 °C. No significant change has been detected. It was below the accuracy of the measurement of 4 fF. For polyurethane based foams, changes are expected at temperatures above 100 °C [48]. Since our sensors aren't used in this range, this effect can be ignored.

3.4.3. Humidity dependence

Relative permittivity ϵ_r of dry air is about 1.0006 and that of water 80. For a relative humidity of about 60% at 20 °C, the water vapor in the air is about 10 g/m³ or 10 ppm. This results in a relative permittivity of

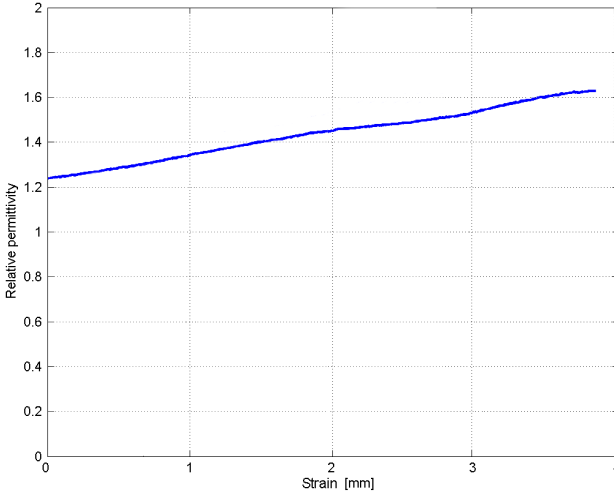


Figure 3.17. Permittivity of the textile spacer depending of the compression.

humid air at 60% of about 1.0014. For the textile spacer the permittivity has been measured for a humid spacer (95% rel. humidity) and no difference has been recorded compared to the capacitance values at about 60% rel. humidity.

If there is condensing humidity and the spacer is wet, changes in permittivity become significant since the amount of water is higher than when no condensing occurs. A completely wet spacer increases the permittivity to that of water, meaning factor 80.

The relative permittivity $\epsilon_r(wet)$ for a wet spacer with relative volumetric content V_w of water is expected as

$$\epsilon_r(wet) = \epsilon_r(dry)(1 - V_w) + \epsilon_r(water)V_w \quad (3.22)$$

If the spacer consists 0.2 % water, $\epsilon_r(wet)$ is expected to be 1.16.

The measured change in capacitance between a dry and a wet sensor can be seen in fig. 3.18. The increase of the permittivity is not constant over the whole compression range since the amount of water also changes due to different fluctuations of air and water out of the

sensor. The amount of water in the sensor was 0.2% in wet state. The measured change in capacitance between wet and dry spacer is 1.19 at zero compression and 1.25 when the spacer is compressed to 30% thickness. After one hour of drying at normal room conditions, a reduction in the measured capacitance towards the dry condition can be recorded.

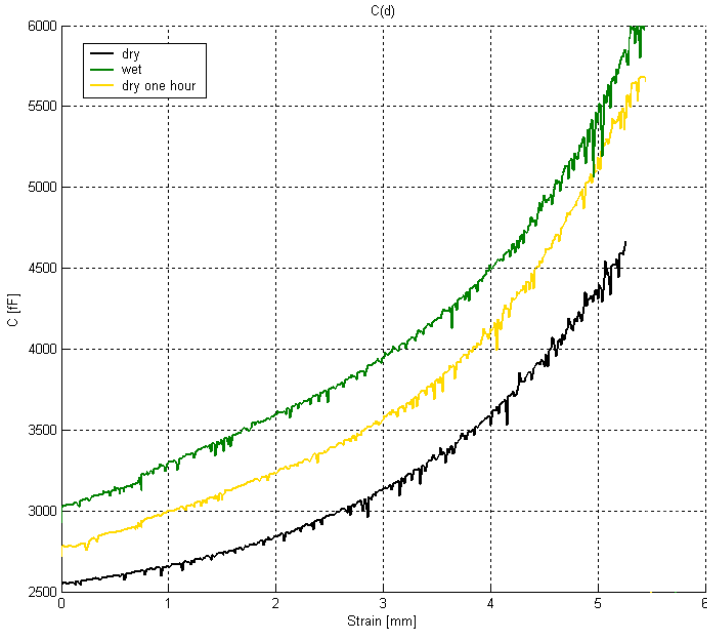


Figure 3.18. Capacitance of a wet sensor compared to dry condition and after one hour of drying.

3.5. Comparison and conclusion

Since the parasitic capacitance is up to a factor of 75 higher than the one of the sensor elements, a measurement method is needed that is insensitive to parasitic capacitance. Two-port measurement is possible with the textile sensor, since there is no need to connect one electrode to ground. Methods that use two-port measuring are: Smart charge redis-

tribution, charge-discharge method, impedance measurement, modified Martin oscillator, multiple sensor modulator and sigma-delta conversion implemented in the AD7745.

Impedance measurements and also the oscillation and resonance methods are sensitive to the resistance of the wires. Impedance measurement can be performed at different frequencies to calculate the ohmic resistance of the wires.

Constant charge operation needs uninterrupted measurement and change of the capacitance since it measures only capacitance changes. This is not the case for the textile sensor and therefore not usable.

Smart charge redistribution is the improved method of the charge-discharge method. With a relative error of less than 250 ppm and a measurement time of 1 ms it fits the requirements (chapter 3.1). The accuracy (250 ppm non-linearity, 15 fF offset) and sampling rate (5 ms) of the multiple sensor modulator is in a comparable range.

The sigma-delta conversion of the chip AD7745 from Analog Devices is a similar method to the smart charge redistribution. The parasitic capacitance of 100-150 pF in the textile sensor induce errors of less than 0.1% within the sensor range of 3-8 pF. A measurement time of 1.1 ms fits the requirements stated in section 3.1.

Methods that fulfill the requirements are the multiple sensor modulator, smart charge redistribution and sigma-delta converter. Since the sigma-delta converter chip offers parasitic compensation, high accuracy in the desired capacitance range, an acceptable sampling rate and is easy to use, it has been selected for the capacitance measuring of the prototypes of the textile pressure sensor.

Changes of the permittivity are not compensated since their influence on the measurement is low enough for induced temperature and humidity variations, and the pressure dependent part is eliminated by calibration. The sensor has to be protected from getting wet, e.g. by covering with Gore-Tex or comparable material.

4

Hysteresis Modeling

Hysteresis is a phenomena occurring in every material when it is bended or compressed. Since the pressure sensor uses compressible materials, hysteresis has to be taken into account. In this chapter we describe the hysteresis in the textile pressure sensor and how it can be modeled to obtain accurate pressure values out of the measured capacitance.

4.1. Hysteresis phenomena in the textile sensor

The compressible spacer between the electrodes provokes hysteresis in the displacement-pressure diagram. For the textile spacer of 6 mm thickness this is illustrated in fig. 4.1. The hysteresis leads to a maximal difference greater than 50% of pressure between the upper and lower branch of the hysteresis curve when a cycle is performed from zero to maximal pressure and backwards. If the pressure is calculated from the mean of the maximal and minimal reachable pressure values at a given strain, the resulting error is in the range of up to 20% to 30%.

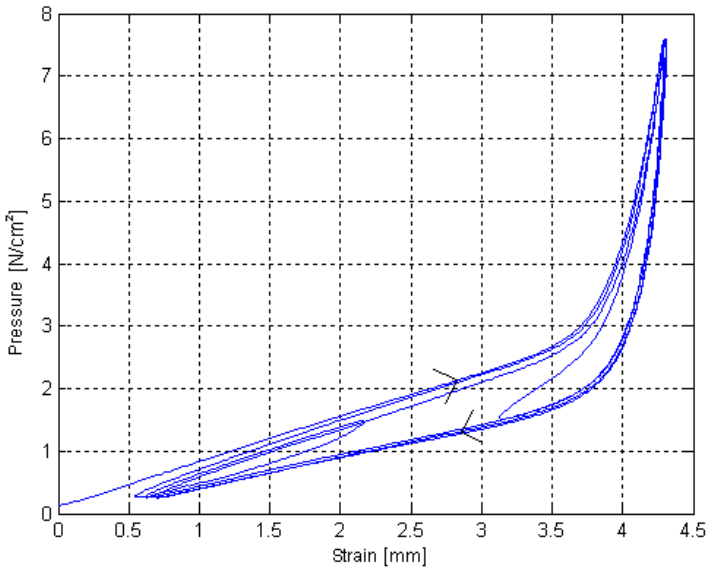


Figure 4.1. Hysteresis in the compression-pressure diagram of the textile spacer with 6 mm thickness.

The hysteresis of different foams varies in distance and shape of their bounding curves and in pressure range as illustrated in fig. 4.2. The analyzed foams have similar characteristics to the textile spacer. The maximal difference of pressure between falling and rising pressure at given strain is in the range of 20% to 60% relative to the value of rising pressure.

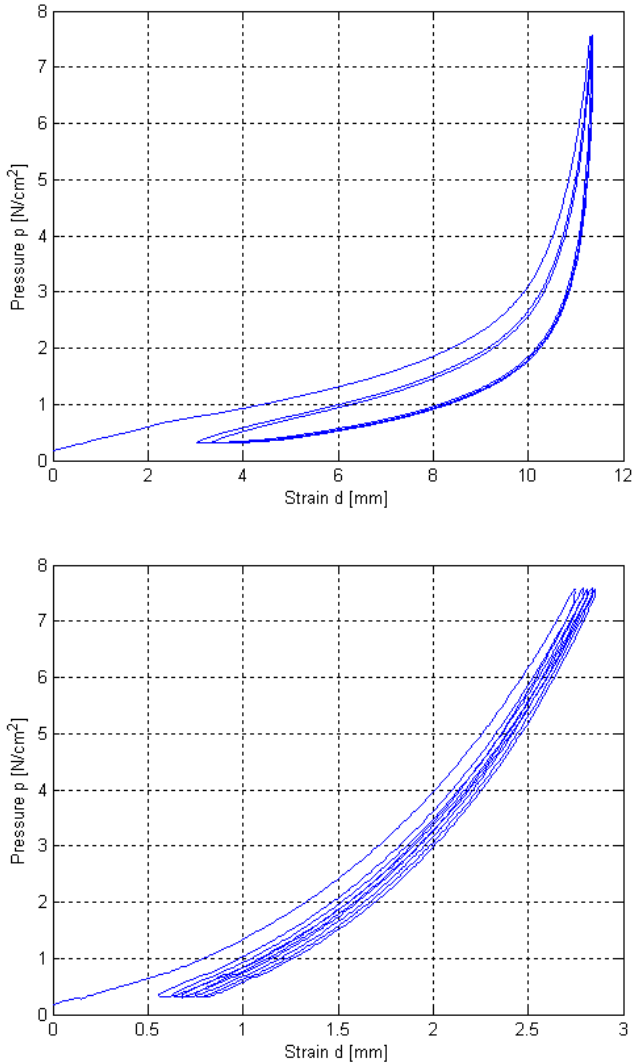


Figure 4.2. The hysteretic behavior is dependent on the spacer material. Shown are hysteresis of a soft, closed cell foam with 13 mm thickness and large hysteresis (top) and another foam of 4mm thickness with small hysteresis (bottom).

The hysteresis curve is not constant over time like in a magnetic material. The distance of the upper and lower bounds of the hysteretic curve depend also on the time and pressure induced. A shift towards higher compression can be observed under load. This is because of drift and that will be discussed in chapter 5.

The speed of pressure change has a minor influence in the hysteresis. Hysteresis has been measured for the textile spacer of 6 mm thickness for different compression speed at 0.1, 1, 10 and 50 mm/min for a compression cycle from 0 to 10 N/cm^2 and back to 0. Differences of the pressure between the force in the range of 0 mm and 4 mm strain are below 2%, while they increase up to 5-10% for higher compression as can be seen in fig. 4.3. The tendency to lower pressure values for increasing speed for the 0.1, 1 and 10 mm/min curves above 4 mm strain is sample dependent as further measurements showed.

To obtain accurate pressure values from the sensor system two possibilities exist: A spacer that shows a small hysteresis can be used as spacer for the textile sensor or the hysteresis can be modeled with a mathematical model to calculate the accurate pressure. The first approach reduces the amount of usable spacers. All the investigated foams and textile spacer provoke an error by the hysteresis that is larger than the 10% specified (Chapter 2.1). Rubber has a hysteresis of a few percent, which is sufficiently small. The disadvantage is that this material is too stiff and not applicable for the desired compression range. Furthermore it would affect the feel of the textile too much because it's rather stiff and airtight which results in non breathable clothing.

Therefore a compensation of the hysteretic error by post processing of the measured data is preferred.

4.2. Causes for hysteresis

The simplest abstraction of a spacer is a spring in parallel with a friction. The friction is causing hysteresis due to energy dissipation in the material while compression is changing. Hysteresis has several reasons.

Friction occurs between the polyester hairs in the textile spacer or the cell walls in a foam and also in the inner molecular structure. The friction force $F_{friction}$ that is directed in the opposite direction of the movement causes the hysteresis (fig 4.4). This effect is completely reversible, which means, that the shape of the hysteresis curve would keep constant over time. In open cell foams and the textile spacer,

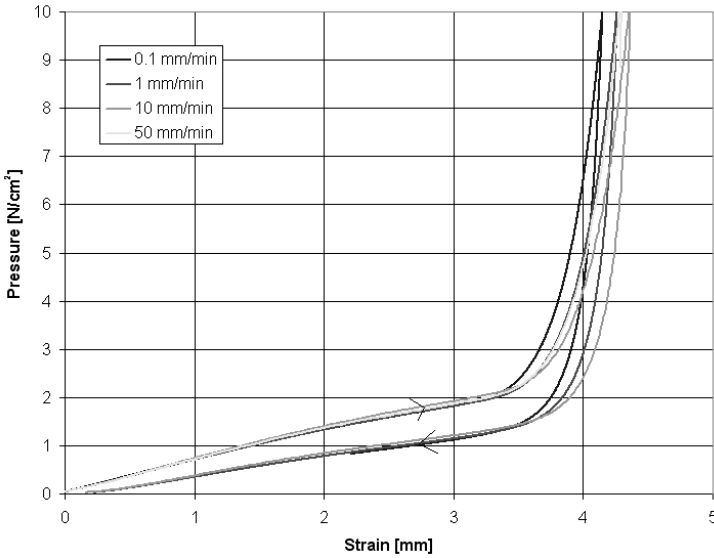


Figure 4.3. Hysteresis of the textile spacer at different speed of pressure change.

friction by dissipation of the gas between the structure increases this effect further.

The force caused by the spacer is also dependent on the pressure distribution over time on the material, due to temporary deformation processes in the molecular structure. Therefore, the hysteresis curve is shifted over time with higher pressure to higher compression since the material becomes thinner. If the pressure decreases, the material recovers and the hysteresis curve is shifted back, so this effect is reversible, too. A non-reversible effect is cracking that prevents the foam to re-expand to the original thickness. The displacement and cracking was analyzed for open cell nickel foams in [23]. These processes take action in the same manner in soft foams but cracking is less frequent under normal stress.

Another non-linearity is that at higher compression, the thickness of the spacer decreases much slower when pressure is increasing. The air gaps are closed at this time and the material is less compressible. In closed cell foams, the non-linear compression of the gas causes a

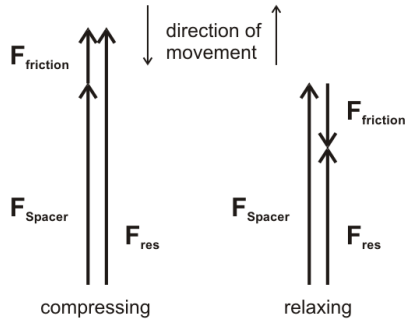


Figure 4.4. Friction force $F_{friction}$ directed in opposite direction of the movement is added to the force from the Spacer without hysteresis F_{spacer} resulting in different force F_{res} for compressing and relaxing.

smoother variation in compressibility.

The described hysteresis behavior has to be implemented in a mathematical model to calculate the appropriate pressure at a given distance between the electrodes.

4.3. Mathematical models for hysteresis

Models are available that describe foam behavior at micromechanical level [10, 105]. Such models are only valid for a particular foam type. Liquid foams have been modeled in [93, 103]. The Gibson model [37] has been used to describe stress-strain relationships in foams [13].

Several mathematical hysteresis models are known in literature. Krasnosel'skii and Pokrovskii [54] invented the hysterons, mainly used to describe magnetic phenomena. The Chua-Stromsmoe model [21] is also commonly used.

The Bouc-Wen Model, originally by Bouc [17] and modified by Wen [115] is known in material science to describe hysteretic behavior. It is able to describe classes of hysteretic curves from magnetic behavior to structures with inconstant stress-strain relationships or seismic excitations [91]. The model is described by [89]

$$\ddot{x}(t) = f(x, \dot{x}, z, u) \quad (4.1)$$

$$\ddot{x}(t_0) = x_{00}, \quad (4.2)$$

$$\dot{z} = A\dot{x} - \beta\dot{x}|z|^n - \gamma|\dot{x}||z|^{n-1}z, \quad (4.3)$$

$$z(t_0) = z_0 \quad (4.4)$$

with $x(t)$ the position of an oscillator at time t , that represents in the case of the pressure sensor the distance between the plates or capacitance. z is a restoring force on the oscillator and the output of the model. The parameters n , A , β and γ control the shape and scale of the hysteretic curve. Hysteretic behavior as well as pressure changes by constant compression can be modeled directly with this model. However, the shift of the hysteresis during longer pressure can't be modeled in this implementation and needs further modification. Moreover further investigations are needed to obtain all the parameters of the model out of a measurement curve.

The Preisach Model [84] is often used for magnetic materials, but it can be applied to mechanics of materials as well. The advantage of the Preisach Model is that only reference curves are needed to define the model parameters; it needs low computation costs so that the model can be implemented into a microcontroller. This model is further used to describe the hysteresis in our system.

All presented models have been applied successfully in general control algorithms for many classes of hysteretic behavior. Detailed descriptions of these models can be found in [89].

4.3.1. Preisach model

The Preisach model [84] is known in the area of magnetics [35, 118] to describe the hysteretic behavior of magnetic material. It has also been used for adsorption hysteresis [32]. Only static hysteresis can be modeled, that means the hysteresis curve keeps constant over time.

The Preisach Model is based on a superposition of an infinite amount of relay operators $\gamma_{\alpha\beta}$. A relay operator is represented by a rectangular loop in the input-output diagram. Its value is either -1 or 1. α and β are the switching numbers where the value of the operator changes by raising or falling input $u(t)$, respectively, as illustrated in fig. 4.5

$$\gamma_{\alpha\beta}(t) = \begin{cases} -1, & \text{if } (t) \leq \beta \\ \gamma_{\alpha\beta}(\max t_M), & \text{if } \beta < u(t) < \alpha \\ 1, & \text{otherwise} \end{cases} \quad (4.5)$$

with $t_M := \tau \in [0, t] | (u(t) \geq \beta \cup u(t) \leq \alpha)$

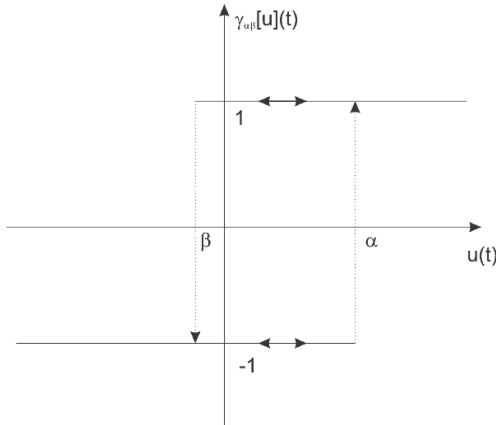


Figure 4.5. Elementary hysteresis operator $\gamma_{\alpha\beta}$

These operators are multiplied with the weight function $\mu(\alpha, \beta)$. The output hysteresis is defined as

$$h(t) = \iint_{\alpha \geq \beta} \mu(\alpha, \beta) \gamma_{\alpha\beta} u(t) d\alpha d\beta \quad (4.6)$$

with $u(t)$ the input, the compression of the spacer in our sensor.

For hysteresis with closed major loops, the function $\mu(\alpha, \beta)$ is restricted to a triangle T on the α, β plane [71]. Outside this triangle $\mu(\alpha, \beta)$ is equal to zero (fig. 4.6).

In a geometric interpretation the relay operators $\gamma_{\alpha\beta}$ have a one-to-one correspondence between points (α, β) in the half plane $\alpha \geq \beta$. The triangle T is divided into two parts. One part $S_+(t)$ consists of points (α, β) where $\gamma_{\alpha\beta} = 1$, and the other part $S_-(t)$ consisting of points for which $\gamma_{\alpha\beta} = -1$.

$$S_+(t) = \{(\beta, \alpha) \in T(\alpha_0, \beta_0) : \gamma_{\alpha\beta}(u(t)) = 1\} \quad (4.7)$$

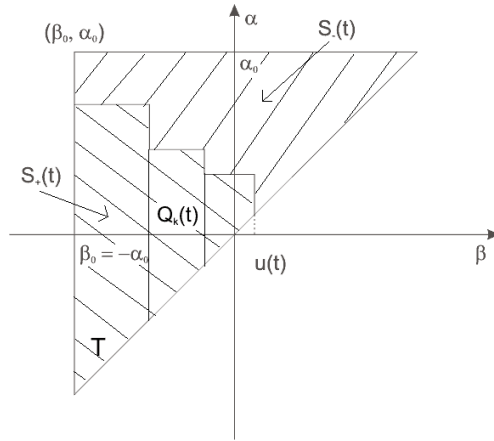


Figure 4.6. For closed loop hysteresis the function $\mu(\alpha, \beta)$ is restricted to a triangle.

$$S_-(t) = \{(\beta, \alpha) \in T(\alpha_0, \beta_0) : \gamma_{\alpha\beta}(u(t)) = -1\} \quad (4.8)$$

The interface between $S_+(t)$ and $S_-(t)$ is a stair line with edge points where the input $u(t)$ has local maxima M and minima m .

As shown in fig. 4.6 $S_+(t)$ can be split into $n(t)$ trapezoids $Q_k(t)$ with $1 \geq k \geq n(t)$ which edges are defined by the local maxima M_k and minima m_k and the input $u(t)$. The model can now be formulated as

$$h(t) = - \iint_{T(\alpha_0, \beta_0)} \mu(\alpha, \beta) d\alpha d\beta + 2 \sum_{k=1}^{n(t)} \iint_{Q_k(t)} \mu(\alpha, \beta) d\alpha d\beta \quad (4.9)$$

The integrals of $Q_k(t)$ can be calculated the following way:

$$\iint_{Q_k(t)} \mu(\alpha, \beta) d\alpha d\beta = \iint_{T(M_k, m_{k-1})} \mu(\alpha, \beta) d\alpha d\beta - \iint_{T(M_k, m_k)} \mu(\alpha, \beta) d\alpha d\beta \quad (4.10)$$

The weight function $\mu(\alpha, \beta)$ can be found from experimentally measured curves. For a point (α, β) in the Triangle T , it can be calculated as [40]

$$\mu(\alpha, \beta) = -\frac{1}{2} \frac{\delta^2 F(\alpha, \beta)}{\delta\alpha\delta\beta} \tag{4.11}$$

with

$$F(\alpha, \beta) = \frac{1}{2}(h_\alpha - h_{\alpha,\beta}) \tag{4.12}$$

where h_α represents the desired output $h(t)$ when $u(t)$ increases from negative saturation to $u(t) = \alpha$. If $u(t)$ decreases afterwards to value β , the output is $h_{\alpha,\beta}$.

4.4. Implementation of the Preisach model

4.4.1. Numerical implementation of the Preisach model

In [51] an algorithm is presented for a numerical implementation of the Preisach model.

The model can be approximated by setting up a equidistant grid over T and discretize t . For every grid point (α_i, β_j) the corresponding value can be calculated as

$$F(\alpha_i, \beta_j) = \iint_{T(\alpha_i, \beta_j)} \mu(\alpha, \beta) d\alpha d\beta \tag{4.13}$$

$$= \frac{1}{2}(h_{\alpha_i} - h_{\alpha_i, \beta_j}) \tag{4.14}$$

$h(t)$ can be rewritten as

$$\begin{aligned} h(t) = & - F(\alpha_0, \beta_0) + 2 \sum_{k=1}^{n(t)-1} [F(M_k, m_{k-1}) - F(M_k, m_k)] \\ & + 2F(M_{n(t)}, m_{n(t)-1}) - F(M_{n(t)}, u(t)) \end{aligned} \tag{4.15}$$

for falling input, and

$$\begin{aligned} h(t) = & - F(\alpha_0, \beta_0) + 2 \sum_{k=1}^{n(t)-1} (F[M_k, m_{k-1}) - F(M_k, m_k)] \\ & + 2F(u(t), m_{n(t)-1}) \end{aligned} \tag{4.16}$$

for raising input.

The values of $F(\alpha_i, \beta_j)$ can be calculated with eq. 4.12 by a reference measurement and stored in a matrix. The output at local extremum have to be stored. Points that are not identical to grid points are linearly interpolated.

Each local minimum m_k of the input is removed from the history if it's larger than the input $u(t)$ when the input is falling. When input rises, all local maxima M_k which are smaller than the actual input were deleted.

It isn't necessary to calculate the sums in (4.15) and (4.16) in each time step. For falling input, $h(t)$ can be rewritten as

$$h(t) = x(t) - 2F(M_{n(t)}, u(t)) \tag{4.17}$$

with

$$\begin{aligned} x(t) = & - F(\alpha_0, \beta_0) + 2 \sum_{k=1}^{n(t)-1} (F(M_k, m_{k-1}) - F(M_k, m_k)) \\ & + 2F(M_{n(t)}, m_{n(t)-1}) \end{aligned} \tag{4.18}$$

$x(t)$ is constant until a local maximum M or minimum m of the input $u(t)$ is generated or deleted. Therefore $h(t)$ can be calculated from the previous values of $h(t)$ with the following case differentiation:

1. Extremum in input at previous time step $t-1$:

$$x(t) = h(t - 1) \tag{4.19}$$

2. Deletion of extremum at time t . t_{M_l} and t_{m_l} are the time of occurrence of the smallest maximum that is larger than the input and the largest minimum that is smaller than the input, respectively:

$$x(t) = h(t_{M_l}) : t_{M_l} < t \tag{4.20}$$

for falling input and

$$x(t) = h(t_{m_l}) : t_{m_l} < t \tag{4.21}$$

for raising input.

3. In all other cases:

$$x(t) = x(t - 1) : x(0) = -F(\alpha_0, \beta_0) \tag{4.22}$$

4.4.2. Declaration of parameter values

The values of the model parameters are defined with measuring pressure depending on the compression (strain) of the spacer. The model parameter $F(\alpha, \beta)$ is calculated according to eq. 4.12 by increasing the input (compression or alternatively capacitance) to the value α . h_α is set to the pressure at this point. Then the input is decreased to the value β and $h_{\alpha, \beta}$ set to the pressure at the new point. Curves starting from h_α down to 0 have to be measured for each α (fig. 4.7). The values α and β are chosen so that the whole desired pressure range is covered.

To define the values of h_α for the textile spacer the pressure on the spacer has been increased from 0 N/cm^2 to 10 N/cm^2 . To define $h_{\alpha, \beta}$, practice has shown that the model is accurate enough, if only three curves for three different α are measured and the remainder are interpolated. For the textile spacer, curves falling from 100%, 70% and 30% of maximal pressure have been recorded. These points have been chosen depending on the shape of the curve. In the region of 70% of maximal pressure the derivative of the pressure with respect to compression is changing as can be seen in fig. 4.7. The starting points of these curves have to be adopted according to the spacer used.

4.5. Results and conclusion

The model has been evaluated by modeling the hysteresis of the textile spacer with 6 mm thickness.

The pressure runs through a cycle from 0 N/cm^2 to 10 N/cm^2 , 1.3 N/cm^2 , 10 N/cm^2 , 0 N/cm^2 , 1.3 N/cm^2 and back to 0 N/cm^2 (fig. 4.8). This cycle has been repeated 50 times continuously with four different samples of the spacer. On the one hand the pressure has been measured by the test machine and on the other modeled with the Preisach model by using the strain as model input.

The modeled and measured pressure curve for one cycle can be seen in (fig. 4.8) and the corresponding error curve in fig. 4.9. By using the Preisach model, the maximal error induced by hysteresis of the textile spacer could be reduced from 50% below 10% between modeled and measured pressure curve in the range of 0.5 to 3.5 N/cm^2 . For higher pressure the maximal error increases to 30%. The average error is around 5% up to 3.5 N/cm^2 and 8% for 3.5 N/cm^2 to 10 N/cm^2 .

The same cyclic test has been performed on the the foams introduced in chapter 2.3.3. The average error is between 8% and 11% and

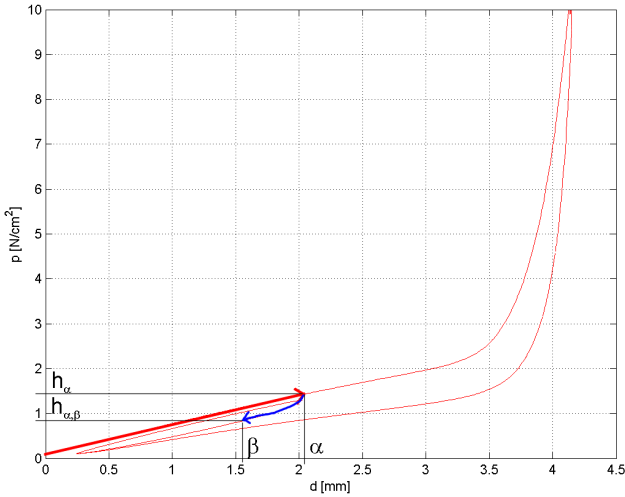


Figure 4.7. Parameter definition of the model. h_α is defined by a rising bounding curve and $h_{\alpha,\beta}$ by falling curves.

the maximum between 11% and 15%.

If the pressure lasts longer and more cycles are performed, the accuracy decreases due to drift, and results in a shift of the hysteresis curve. Furthermore, the changes of pressure when the compression is held constant, lead to a higher error that is above 10%. The foam with the largest drift already produced an error up to 100% after a few dozen cycles. Therefore further modeling is needed to reduce drift errors. This will be discussed in the following chapter.

From these results we can state that the required accuracy of 5% in average (chapter 2.1) can be reached by modeling the hysteresis with the presented model for cyclic pressure change up to a duration of two hours. The model can also be used for other than the analyzed spacers, only the calibration curves have to be recorded. It is also possible to use it for other types of sensors where a force-strain behavior can be measured, e.g. for elongation sensors.

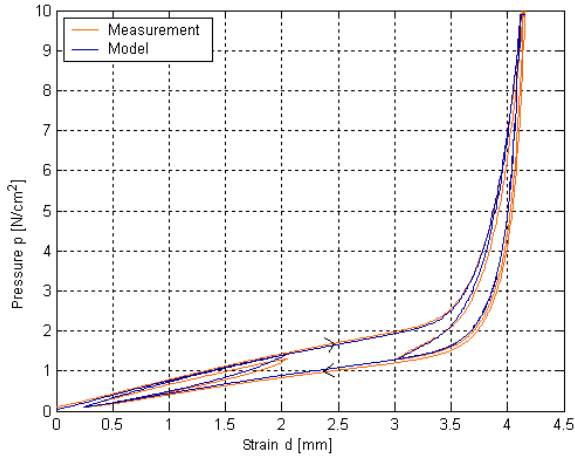


Figure 4.8. Pressure p from the output of the model compared to the measured pressure dependent on the compression d

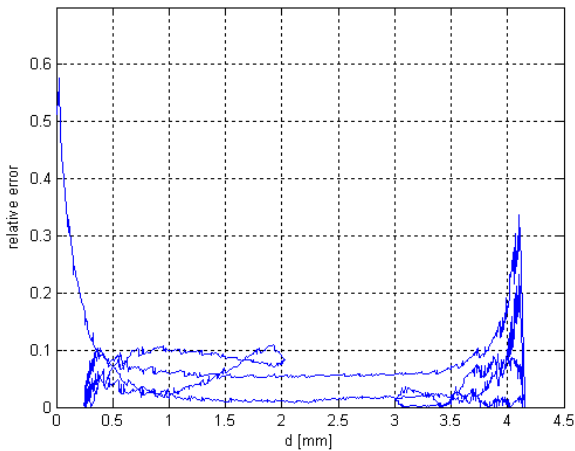


Figure 4.9. Relative error of model output compared to the measured pressure dependent on the compression d for three different cycles (same cycles as in fig 4.8).

5

Drift Compensation

Drift is an additional error source in sensors. In this chapter we describe the drift phenomena in the textile pressure sensor and show how it can be modeled.

5.1. Drift behavior of the textile pressure sensor

5.1.1. Characterization of drift

In the last chapter we introduced the simplified abstraction of a spacer by a spring f and a pad r causing friction in parallel. The spring factor of f in a spacer is not only a function of the actual compression, but also of the pressure induced in the past. This degradation of f causes drift. This can also be interpreted as another spring f_s in series to f and a spring f_p in series to a damper d in parallel (fig. 5.1) [47].

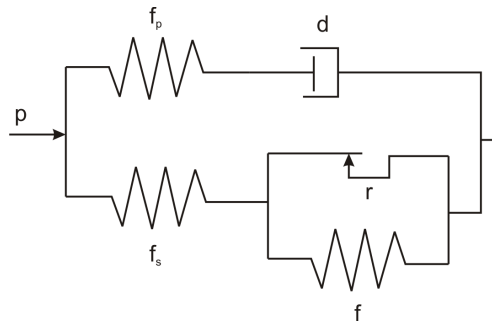


Figure 5.1. Simplified model of a spacer.

Drift in a spacer occurs in two ways. On the one hand when the compression (thickness of the spacer) is held constant after an initial change of pressure on the spacer, the pressure changes further over time. On the other hand, when repetitive cycles of compressing and relaxing of the spacer are performed, the pressure is different between the cycles at the same points of compression and same sign of derivation of compression (fig. 5.5).

The structure of the spacer material is changing while load is applied. Microscopic and macroscopic effects are involved. Hysteresis and drift have similar causes that are the reason for both effects. The difference of the two phenomena is defined more by their effects, drift can occur by constant input while hysteresis only by variable input.

At the macroscopic side, structures in the spacer that are stuck together lose their contact and slip away, which results in lower counterforce. Such structures can be the polyester pile yarns in the textile spacer or the cells in a foam (chapter 2.3.3). In an open cell foam or

in the textile spacer, exhaust of air from the structure results also in a short time drift. Depending on the resistance to exhausting the air, this effect can be seen during the range of milliseconds (textile spacer with its open structure) to seconds (little porous foam). Breaks of the structures in the spacer are another source of drift. Unlike the effects mentioned before, this one is not reversible and leads to permanent deformation.

Microscopic effects occur in the inner molecular structure of a spacer [83]. Connections between molecules are reordered to a lower potential energy.

When these effects occur instantly while the pressure is varying, they cause hysteresis; when they occur at random time after the igniting event, they cause drift.

5.1.2. Measurements

Drift for constant compression has been measured for the textile spacer (chapter 2.3.3) by measuring the step response.

Theoretically, raising the pressure during the step should be infinitely fast (definition of a step). With the test machine used the maximal speed that could be reasonably performed is 50 mm/min. One step takes between 2 and 5 seconds.

5.1.2.1. Drift during constant compression

The spacer has been compressed from zero pressure to a defined value and then the compression has been held constant for one hour and the pressure measured over time. Step sizes s were: 2.5, 5.0, 7.5 and 10 N/cm^2 . As can be seen in fig. 5.2, the curves for each initial pressure are similar. That means, the change of pressure Δp at a certain time t after the step is approximately proportional to the step size s

$$\Delta p(t) \sim s \tag{5.1}$$

The difference Δs between exact proportionality (eq. 5.1) and the measured pressure relative to s at a certain time t is below 4%.

The same drift behavior also has been observed for steps from a certain pressure p_2 up to 10 N/cm^2 . The compression before starting the step has been held constant for one hour. For this test Δs is increasing to 21%. For higher initial pressure and therefore lower step size, Δp is higher than expected by proportionality. This can be explained because

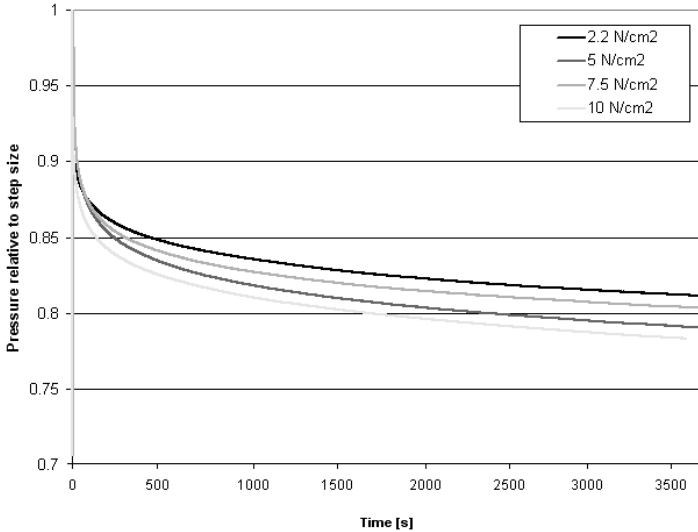


Figure 5.2. Drift of the textile spacer for constant compression for steps from 0 to 2.5, 5.0, 7.5 and 10 N/cm^2 during one hour (normalized to the step size)

the spacer is not yet in steady state after the first step from 0 to the initial pressure, before the second step after one hour is performed. If the time between the first step and second step is increased to five hours, Δs is 12% and therefore proportionality is better. In fact, measuring the step from a certain pressure $p_1 > 0$ to p_2 at time t , the step is a superposition of a step 0 to p_1 at time 0 and p_1 to p_2 at time t .

The same behavior can be observed for falling pressure. Records of steps from 10 N/cm^2 to 0.25, 2.5, 5.0 and 7.2 N/cm^2 show also a similarity between the curves (fig. 5.3).

5.1.2.2. Drift during cyclic compression

Drift can also be seen when cyclic compressions of the spacer are performed. During one cycle the compression has been linearly increased from zero until a defined pressure value p_3 is reached. Afterwards it has been decreased in the same manner. As p_3 2.5, 5.0 and 7.5 N/cm^2 has

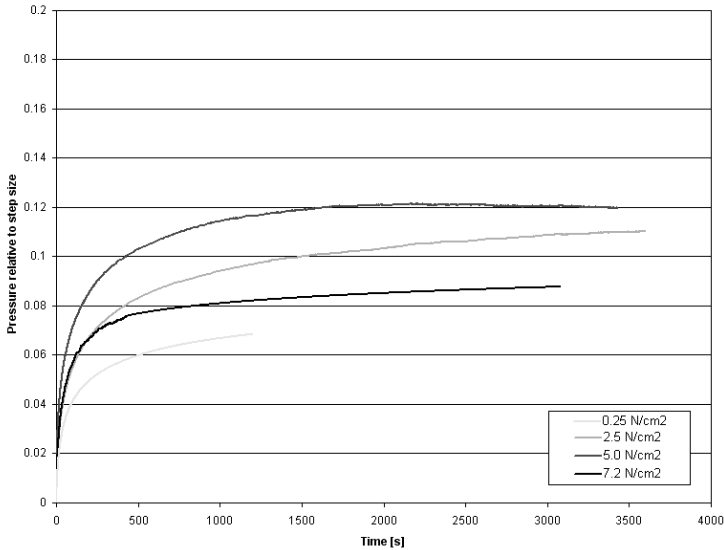


Figure 5.3. Drift of the textile spacer for constant compression for steps from 10 N/cm^2 to 0.25 , 2.5 , 5.0 and 7.2 N/cm^2 (pressure change after the step normalized to the step size)

been chosen.

This results in a hysteresis curve that is shifted towards higher compression when the average pressure before the cycles was lower than during the cycles (or vice versa) (fig. 5.4). The maximum compression reached in one cycle with maximum pressure p_3 can be seen in fig. 5.5.

The hysteresis shift can be seen as a superposition of the cycles with a step response from the origin pressure to the average pressure during the cycles; in the measured cases from 0 to 1.25 , 2.5 and 3.75 N/cm^2 respectively.

5.2. Modeling and compensation of drift

A logarithmic regression of the drift curve has been found empirically from the step responses. The pressure $p(t)$ after a step at time t_0 with size s is:

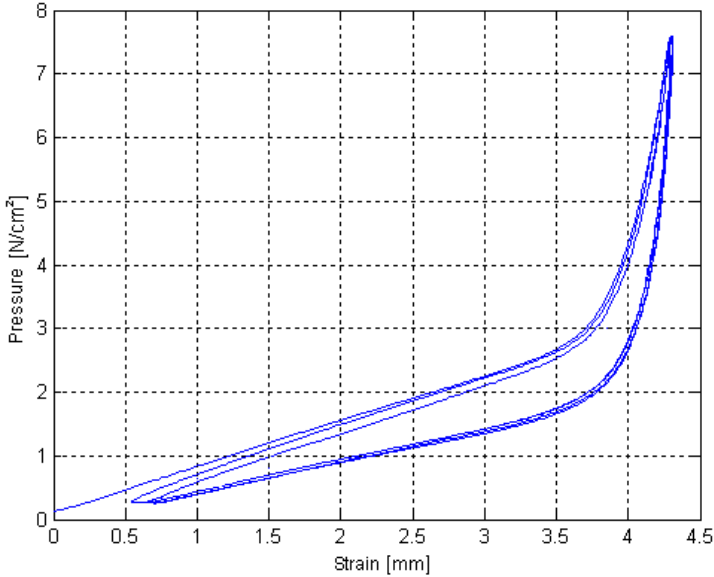


Figure 5.4. Hysteresis curve is shifted towards higher compression when cyclic compression is applied to a recovered textile spacer.

$$p(t) = s\gamma \ln(t - t_0 + 1) + p(t_0) \text{ for } t \geq t_0 \quad (5.2)$$

where $p(t_0)$ represents the pressure right after the step. γ is a scaling factor that defines how fast the pressure decreases. The value of γ depends on the spacer used. It can be evaluated with a second point on the curve at time $t_c > t_0$ with measured pressure $p(t_c)$:

$$\gamma = \frac{p(t_c) - p(t_0)}{s \ln(t_c - t_0 + 1)} \quad (5.3)$$

For one step the curve can be fitted with a maximal error below 1.0% (fig. 5.6). If a common factor γ for all steps from 0 to 2.5, 5.0, 7.5 and 10 N/cm^2 is used, the error increases but the maximum keeps below 4.0% (fig. 5.7).

These curves are valid for one step each. To model drift for real march of pressure, a superposition of the step responses is needed. The

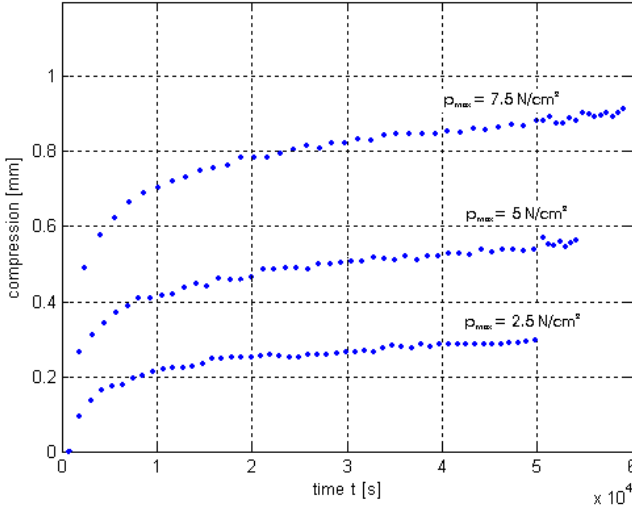


Figure 5.5. Maximum compression for cyclic compression between 0 and 2.5, 5.0 and 7.5 N/cm^2

time t is discretized and the step height calculated as $s(t) = p(t) - p(t-1)$. Since the pressure change after a certain time is proportional to the step size s (eq. 5.1) the step responses can be added. The drift model is given by

$$p(t) = \gamma \sum_{t_i} [(p(t_i) - p(t_{i-1})) \ln(t - t_i + 1) + p(t_i)] \quad (5.4)$$

t_i represents the time where a step occurred. This sum has to be recalculated for every time step. To reduce computation complexity, either the time intervals can be extended or steps with low influence on the sum can be deleted from the history. Such a step can be one that is small compared with a previous one or a step that was a long time ago in the past. To quantify when a deletion of a step has to be performed, we can calculate for each step at time t_i the deviation of the corresponding drift curve. If the ratio between the deviation of the step k at time t_i and the largest deviation over all steps at time t_i is

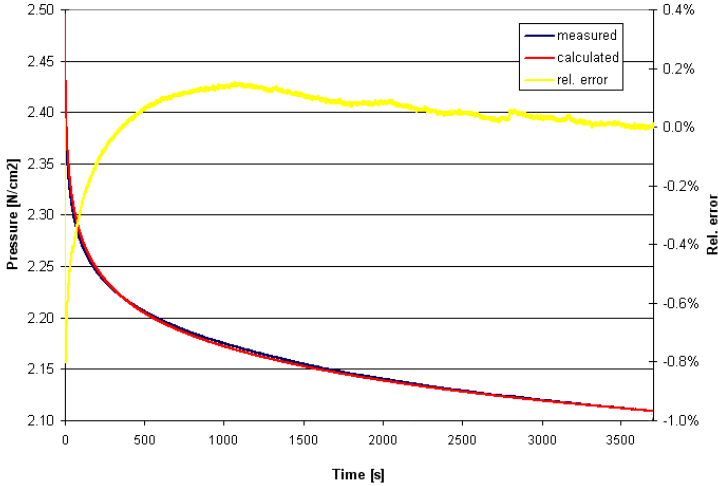


Figure 5.6. Measured and calculated pressure during one hour for a step from 0 to 2.5 N/cm^2 . The difference between the curves is below 1.0%.

smaller than δ , a deletion is performed. Increasing the value of δ would lead to more deletions and less computing power but also less accuracy.

The algorithm is the following: Perform a deletion of step k at time t_i if

$$\frac{\dot{st}(k)}{\max(\dot{st}(n))} < \delta \quad (5.5)$$

with

$$st(x) = (p(t_x) - p(t_{x-1})) \ln(t_i - t_x + 1) \quad (5.6)$$

and

$$n \in [0, i] \quad (5.7)$$

For longer time steps than about one second, it is recommended not to use the actual pressure at each time t_i to calculate the step size. To use the average over a window between t_{i-1} and t_i is more accurate.

5.2.1. Implementation

Drift in the textile sensor is compensated by combining the hysteresis model discussed in the chapter before with the drift model (eq. 5.4).

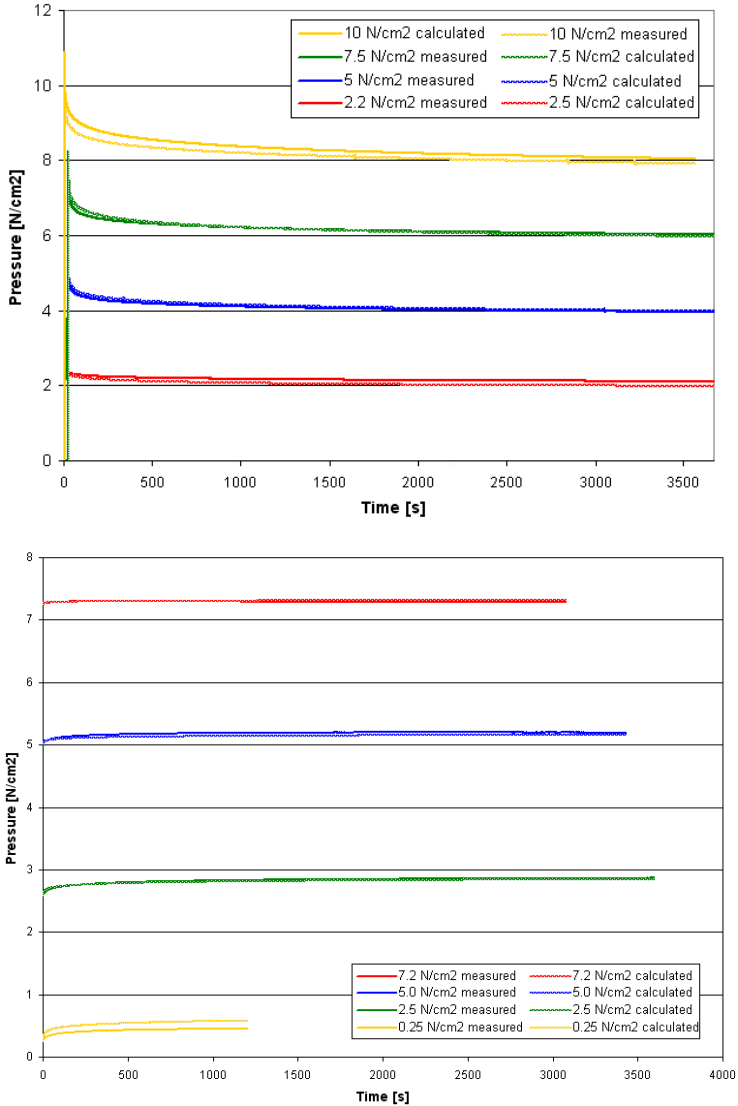


Figure 5.7. Measured and calculated pressure during one hour for steps from 0 to 2.5, 5.0, 7.5 and 10 N/cm^2 (top) and for falling steps from 10 to 7.2, 5.0, 2.5 and 0.25 N/cm^2 (bottom).

As can be seen from the cyclic compression experiment, the hysteresis curve is scaled along the compression. This scaling can be implemented into the hysteresis model by using the output of the hysteresis model $h(t)$ as input of the drift model:

$$p(t) = \gamma \sum_{t_i} [(h(t_i) - h(t_{i-1})) \ln(t - t_i + 1) + h(t_i)] \quad (5.8)$$

5.3. Results and conclusion

For testing the model, we used time steps of 10 seconds. At each time step the difference between the average of the past 10 seconds from the Preisach model output and the average of the 10 seconds prior to the last step has been calculated. If this difference was below 1% this step was omitted. Otherwise the actual pressure $p(t_i)$ and the time t_i were stored and used for the calculation of the sum (eq. 5.8).

The relative error e_r without drift compensation increased above 10% after one hour of cycles (chapter 4.5). With the drift model it reduced to an average below 5.0% for a cyclic compression of the textile spacer during four hours (fig. 5.8). Four different samples have been measured twice. They have been unloaded for several hours before each measurement.

The drift model can further reduce the errors of the measured pressure. A simple model based on logarithmic regression has been found. The pressure can be described by a superposition of previous step responses. Only one factor (γ) has to be measured from the spacer as model parameter.

To use the model for other spacers than the researched one needs further investigation in case the pressure change at a certain time after a step is not proportional to the step size s . Then the summation of the step responses isn't possible anymore and a more complex model has to be found. The drift model has also been tried for reducing drift error in a commercial pressure mat of *Tekscan*. Unfortunately the proportionality to the step size s is not given and the developed drift model can't be used for that purpose.

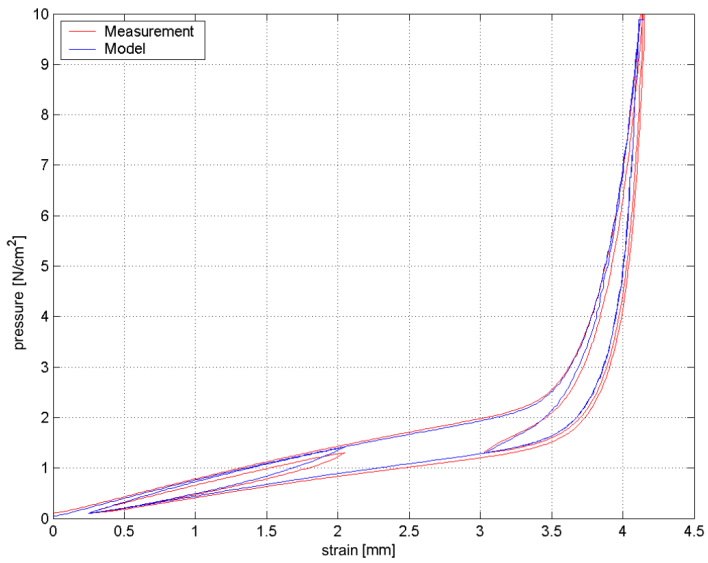


Figure 5.8. Measured and calculated pressure during cyclic compression.

6

Error Modeling

The influence of different error sources such as hysteresis, drift, noise and sensor failure has been modeled and measured for the classification of sitting postures. In the first part of this chapter, the modeling based on adding errors on reference pressure patterns is described. In the second part, these results are validated with the classification of measured sitting postures of nine subjects.

6.1. Introduction

Besides the already discussed error sources such as hysteresis and drift, other errors occur in the textile pressure sensor like noise or sensor failure. The question arises, what is the impact of such errors on a concrete application. Have these errors a significant influence and do they have to be compensated or can they be neglected? How well is the developed textile sensor performing compared with a commercial solution from *Tekscan*?

The detection of sitting postures by classifying pressure patterns on a seat has been used as measure for the quality of the developed sensor system. The textile sensor array with 240 elements has been used for the experiment with a subset of 96 elements selected.

The influence of the error sources hysteresis, drift, noise and sensor failure has been modeled on the one hand, and measured with an experiment on the other hand. The pressure pattern of nine subjects sitting on a chair have been recorded for 16 different postures.

The related work for estimating sitting posture is mentioned in the introduction of this thesis (chapter 1).

6.2. Measurement

6.2.1. Experiment setup

For the experiment the pressure mat with 240 sensor elements has been used while 96 of them were active (fig. 6.1). The remaining sensor elements have been connected to the shield potential (chapter 3.3). The elements are chosen so they cover the whole buttock of each test subject, forming a checkerboard pattern with an overall size of 35 x 40 cm. Using 96 sensors results in a measurement time of 1.6 s for the whole mat. This is a useful value while 4 s would be needed for the whole 240 sensors. Increasing the number of sensors does not necessarily increase the recognition rate [76]. Therefore 96 sensors are a good compromise between resolution and speed.

A commercially available pressure mat from *Tekscan* has been placed below the textile sensor for reference. This mat measures the pressure on the seat with 1024 sensors 20 times a second at a relative accuracy e_r of 10%. The mat has been calibrated before use with the calibration system from *Tekscan* in the range of 0 to 3.3 N/cm^2 . Placing the reference sensor below the textile mat does not influence the pressure distribution over the textile sensor.



Figure 6.1. Textile sensor with 240 elements used for sitting posture measurement. 1: Common electrode, 2: Spacer, 3: Sensing electrodes, 4: Grounded electrodes

Both sensor systems have been mounted on a wooden swivel chair with a flat surface. The height of the chair has been adapted to the length of the legs of the subjects, so that, while sitting upright, their heels are touching the floor and their legs the front of the seat.

6.2.2. Experiments

The following 16 postures have been measured for each subject (fig. 6.2): Seated upright (1), leaning right (2), left (3), forward (4) and back (5), left leg crossed over the right (6) and right over left (7) once seated upright and once leaning back (8,9) once while the knees are touching and once with the ankle rested on the leg (10-13), slouching (14), sitting on the leading edge (15) and slouched down (16). For postures without leaning back the back of the chair isn't touched. Each posture has been held for 30 s. A home position (sitting upright) has been adopted for 5 s between each succeeding position to define the transitions between the postures. Examples of patterns measured by



Figure 6.2. 16 different sitting postures have been performed (for numbers see text).

the *Tekscan* system can be seen in fig. 6.3 and those of the textile sensor in fig. 6.4

The experiment has been conducted with 9 subjects (6 male and 3 female) in three rounds. In each round, each position beside the home position has been taken once. During the first two rounds, the subjects kept permanently sitting on the chair. Between the second and third rounds the sensor has been unloaded for 30 minutes. The unloading guarantees that the sensor completely recovers to ensure the same starting conditions between the first and third round. Therefore drift effects shouldn't be seen between the first and third round, while it can

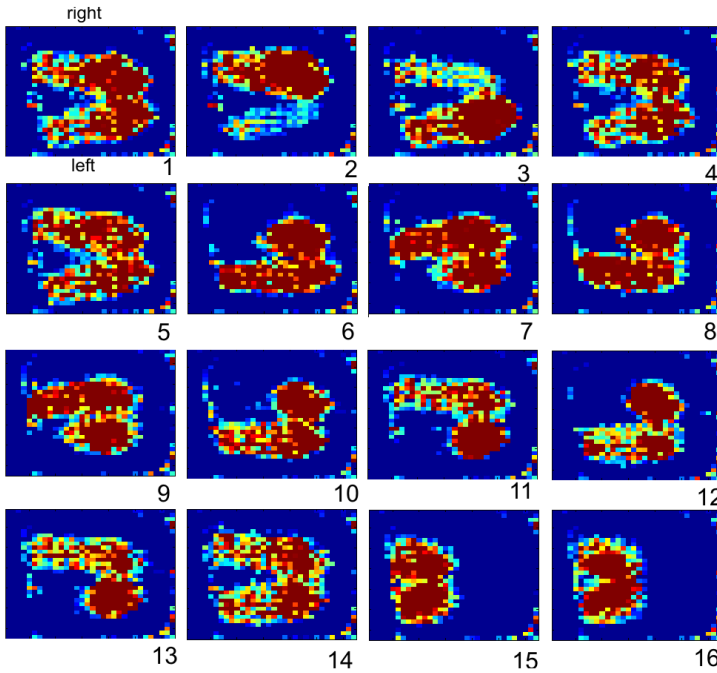


Figure 6.3. Pressure patterns for 16 sitting postures measured with the Tekscan system (for numbers see text).

be measured between the first and second round.

6.3. Classification

6.3.1. Learning algorithm

As learning algorithm naive Bayes classifier has been used [26]. It is based upon the Bayes' theorem. The probability of a class c with a feature set (f_1, \dots, f_n) is given by

$$p(c|f_1, \dots, f_n) = \frac{p(c)p(f_1, \dots, f_n|c)}{p(f_1, \dots, f_n)} \quad (6.1)$$

Because $p(f_1, \dots, f_n)$ is independent on c and equal for all classes, the model can be rewritten to

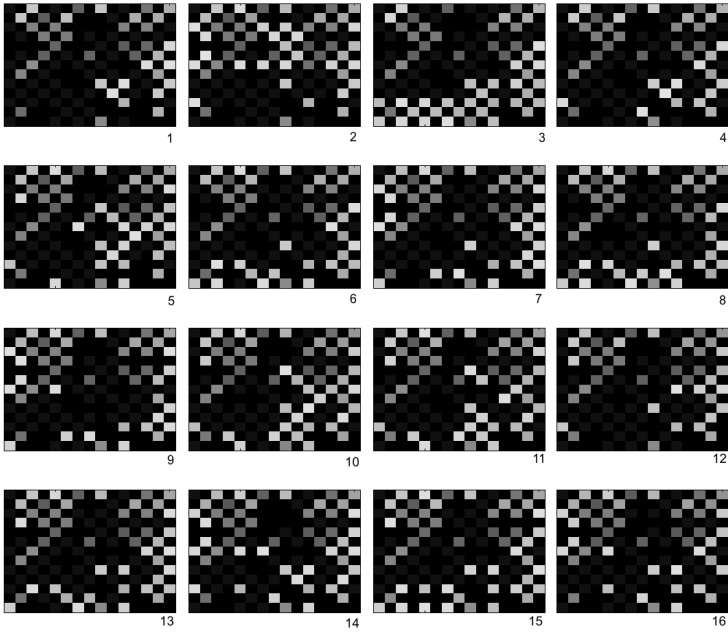


Figure 6.4. Pressure patterns for 16 sitting postures measured with the textile pressure sensor (for numbers see text).

$$p(c, f_1, \dots, f_n) = p(c)p(f_1, \dots, f_n|c) \quad (6.2)$$

Using repeated applications of the definition of conditional probability it can be expressed as:

$$p(c, f_1, \dots, f_n) = p(c)p(f_1|c)p(f_2, \dots, f_n|c, f_1) \quad (6.3)$$

$$= p(c)p(f_1|c)p(f_2|c, f_1)p(f_3, \dots, f_n|c, f_1, f_2) \quad (6.4)$$

$$= p(c)p(f_1|c)p(f_2|c, f_1)p(f_3|c, f_1, f_2) \\ p(f_4, \dots, f_n|c, f_1, f_2, f_3) \quad (6.5)$$

Based on the assumption that each feature f_i is independent on every other feature f_j , $j \neq i$

$$p(f_i|c, f_j) = p(f_i|c) \quad (6.6)$$

the joint model can be written as

$$p(c, f_1, \dots, f_n) = p(c) \prod_{i=1}^n p(f_i|c) \quad (6.7)$$

The so called maximum likelihood estimator to classify the the data is then given by

$$c = \operatorname{argmax}_c p(c) \prod_{i=1}^n p(f_i|c) \quad (6.8)$$

6.3.2. Features

The following features have been tested for classification:

- sensor value from each sensor element
- center of force
- pressure applied to 4 equal aggregated areas of the seating area
- pressure applied to 16 equal aggregated areas of the seating area

A reduced feature set of k-best features has been evaluated with the sequential forward selection (sfs) algorithm [52]. A flow chart of this method can be seen in fig. 6.5. The sfs algorithm starts with an empty feature set $X_0 = \emptyset$. In each step, the feature is added to the existing set X_k that generates highest classification accuracy in addition to X_k . The algorithm is terminated when the desired number of features is selected.

As cost function J the mean of the classification accuracy of the cross validation over all subjects (leave-one-person-out) has been used. The number of features is chosen so that highest classification accuracy has been reached.

The following 16 best features have been found (fig. 6.6):

- values of sensor elements number 9, 10, 16, 31, 34, 38, 39, 56, 62, 65, 86, 89, 91 and 96
- x-coordinate of center of force (sidewards)
- one of the 16 equal aggregated areas (no. a7)

The optimal feature set is used for both, classification of the postures with modeled errors and the measured sitting patterns.

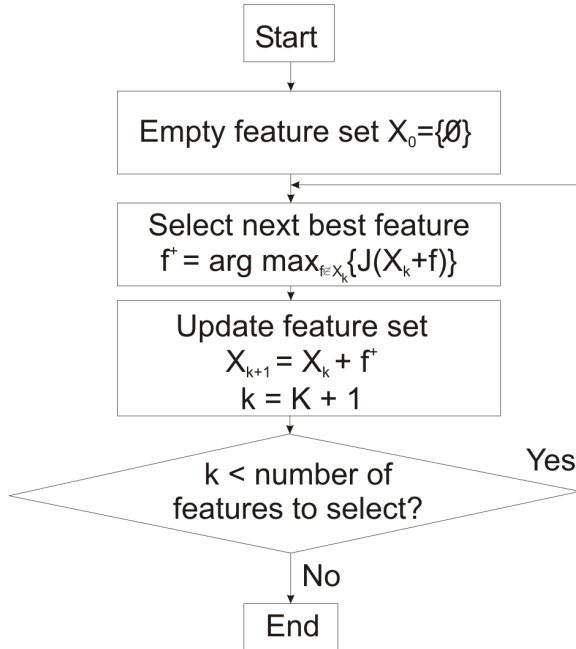


Figure 6.5. Flow chart of the sequential forward selection (sfs).

6.4. Error modeling

6.4.1. Reference patterns

One pressure pattern is defined for each posture as a reference. These patterns are a superposition of different real static measurements of each posture by averaging over several frames. Each posture has only one corresponding pattern, thereby eliminating the influence of different positions, movements and subjects.

32 training patterns are generated out of each reference pattern for use as training patterns (fig 6.7). These training patterns are generated by adding noise to the reference pattern. The noise increases the variance of the training data. A large standard deviation of the noise enhances the robustness of the classifier but on the other hand results in overlapping the sample clouds of the classes and that reduces the accuracy. A standard deviation of $0.05N/cm^2$ still guarantees a

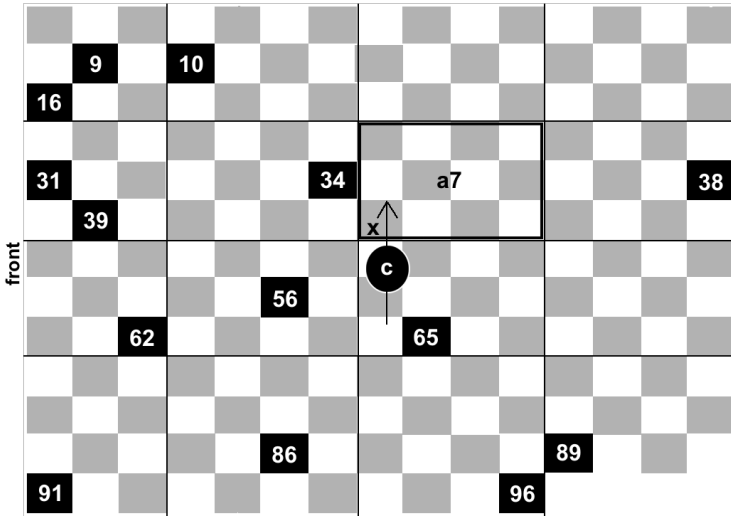


Figure 6.6. 16 best features selected by sfs algorithm (black: selected sensor elements, c: center of force, a7: selected area, grey: available sensor elements).

classification accuracy of 100% when 8-fold method is used within the training patterns.

The reference patterns are recorded with the reference pressure measuring system from Tekscan. Each 2x2 sensor elements of 1024 are averaged to one element resulting in 256 elements in total.

The reference patterns act as basis for research on the influences of the errors. The mentioned error sources are added to the reference patterns creating new patterns. For each posture 15 new patterns are generated that are used as test data.

Each source has a variable parameter to define the influence of the specific error. The classification accuracy and distance between the posture classes are taken as the measure. The same features and algorithms are used as for classifying the measured data. The patterns with errors serve as test data.

6.4.2. Distance between pressure patterns

As a measure of how well a classifier can perform [26], the Mahalanobis distance [66] $d_{i,j}$ between the mean of the samples of classes c_i and c_j

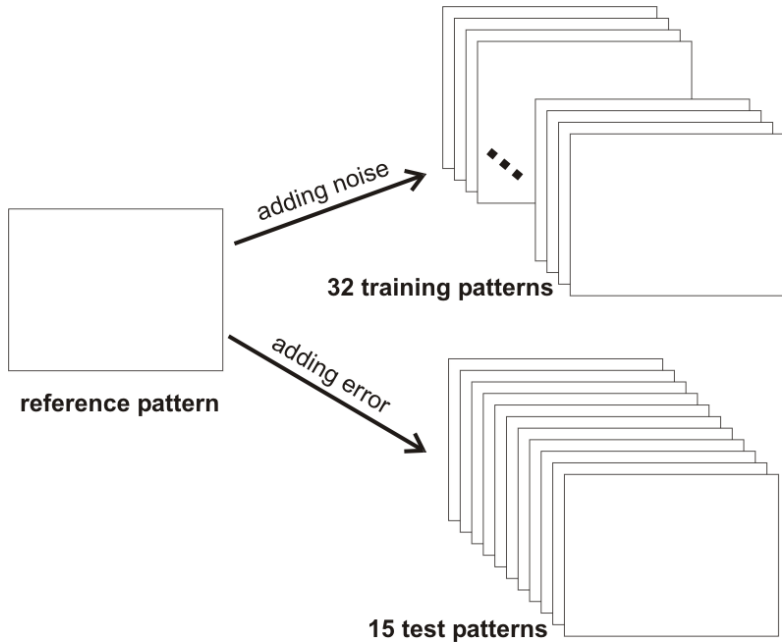


Figure 6.7. Generation of 15 test and 32 training patterns out of a reference pattern for one posture.

with $i \neq j$ has been calculated for all 16 classes. The pressure of the sensor elements has been normalized to the mean of the pressure over the sensor mat.

For all distances between different classes c_i, c_j the average distance d_{md} has been calculated according to

$$d_{md} = \frac{1}{n(n-1)} \sum_{i \neq j} d_{i,j} \quad (6.9)$$

Additionally, the mean distance d_c between the samples within one class c has been calculated. It has been evaluated by the mean of the Mahalanobis distances $d_{k,l}$ between all samples $k \in c$ to all samples $l \in c$:

$$d_c = \frac{1}{n_s(n_s - 1)} \sum_{k,l \in c} d_{k,l} \quad (6.10)$$

with n_s the amount of samples of class c . The average distance d_{ms} has been calculated over all distances d_c for the 16 classes

$$d_{ms} = \frac{1}{n} \sum_{c=1}^n d_c \quad (6.11)$$

with n the number of classes.

d_{ms} and d_{md} have been evaluated against the variable parameter of the corresponding error source.

The distance of the samples within class c can be taken as measure of the 'size' of the sample clouds of c . The classes are perfect separable if the clouds are as small and the distances between the classes high such as the clouds don't overlap.

6.4.3. Noise

To research the influence of noise, gaussian noise is added to the reference patterns. 15 patterns with noise have been generated for each posture as test patterns. The standard deviation of the noise is used as the variable parameter. It is assumed that the noise is uncorrelated between the sensors. Correlated errors are present in the real system of the textile sensor, but they mainly appear as an offset. Offset can be easily reduced by calibrating the sensor and therefore is not investigated further.

6.4.4. Hysteresis

Hysteresis is added to the reference patterns with the Preisach model discussed in chapter 4 for generating the test patterns. Since hysteresis is a phenomenon that occurs only on pressure changes, the hysteresis can't be added directly to the static pressure images. The transitions between the postures are used for defining the hysteresis (fig 6.8).

Test patterns have been generated for the transitions from each posture to each other. The pressure of each sensor element i of the test pattern t_2 is calculated with the hysteresis model. The model is initialized with the pressure p_{i,r_1} of element i of the reference pattern r_1 . r_1 is the pattern of the start of the transition. The input and output $h(p_{i,r_1})$ of the model are identical and equal to p_{i,r_1} . The input is then

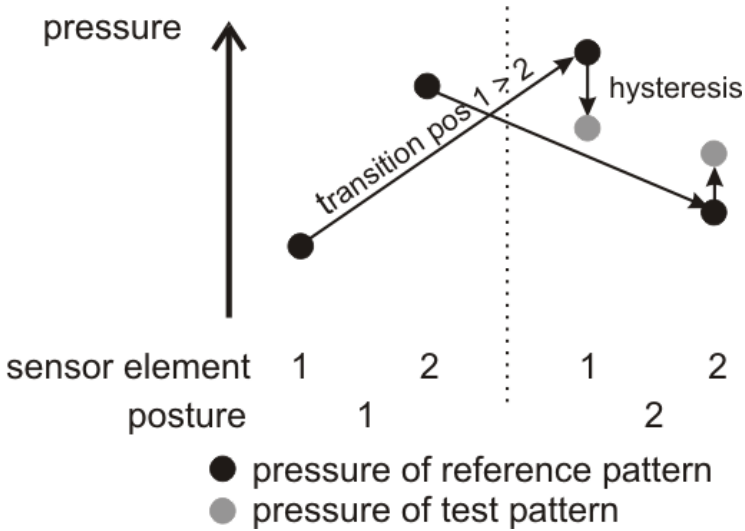


Figure 6.8. Training patterns with hysteresis are generated from the transitions between the postures.

altered to $p_{i,r2}$, the pressure of element i of the destination pattern r_2 of the transition. The output of the hysteresis model $h(p_{i,r2})$ is then the pressure of element i of the test pattern t_2 .

As variable parameter the distance d_h between the upper and lower limiting branches of the hysteresis curve at half pressure range is used. If d_h is zero, the model output $h(p_{i,r2})$ is identical to $p_{i,r2}$ and the test pattern t_2 are identical to the reference pattern r_2 . One way of implementing this scaling is by redefining the model parameters according to d_h . As a less computational complex alternative, one can define the parameters of the hysteresis model for a defined distance d_d . The hysteresis is then scaled with $f_h = d_h/d_d$.

The pressure $p_{i,t2}$ of sensor element i of the test pattern t_2 with the scaling is calculated according to

$$p_{i,t2} = p_{i,r1} + f_h(h(p_{i,r2}) - p_{i,r1}) \tag{6.12}$$

with $h(p_{i,r2})$ representing the hysteresis model.

15 patterns are generated per posture and factor d_h using as test data.

6.4.5. Drift

As discussed in chapter 5 drift in the textile spacer at a time t after a step is proportional to the pressure step. Changing between two postures can be seen as a step for each sensor element since the duration of the posture change is less than a few seconds. To add artificial drift to the ideal pressure pattern, the pressure difference $p_{i,r2} - p_{i,r1}$ between each sensing element i is taken as a step. The pressure $p_{i,t2}$ of the sensor i of the test pattern i is then

$$p_{i,t2} = pr_{i,r2} + (pr_{i,r2} - pr_{i,r1})\gamma \ln(t + 1) \quad (6.13)$$

using the model introduced in chapter 5. The parameter γ is defined by eq. 5.3 and its value is -0.025 for the textile spacer. The time t is used as variable parameter.

15 patterns are generated per posture and time t .

6.4.6. Sensor failure

Sensor signals can be lost mainly due to shortcuts between the electrodes and wiring. The question we want to answer is, how many sensors can fail to guarantee a defined classification accuracy. A defined amount f of randomly chosen failing sensors is set to zero. A different set of failing sensors is chosen for each test pattern.

6.5. Results

6.5.1. Classification from modeled patterns

The features calculated from the reference patterns with 256 sensor elements have been used as training data and the test patterns with added errors as test data.

The distances between the classes and within the classes have been calculated according to section 6.4.2.

6.5.1.1. Noise

The measured pressures while sitting on the chair with the reference system are in the range of 0 to 5 N/cm^2 . The standard deviation of the added noise to the reference patterns for generating the test patterns is increased from 0.013 N/cm^2 up to 1.3 N/cm^2 , that is 0.3% to 30% of the whole measured range.

Up to a standard deviation of 0.55 N/cm^2 , the recognition rate keeps around 100% (fig. 6.9). This standard deviation corresponds to 12% of the full pressure range measured. The recognition rate drops significantly for a standard deviation of above 0.68 N/cm^2 . Increasing the noise level up to 1.1 N/cm^2 leads to a drop of the rate below 15%. For higher values of the standard deviation, the recognition rate decreases slower.

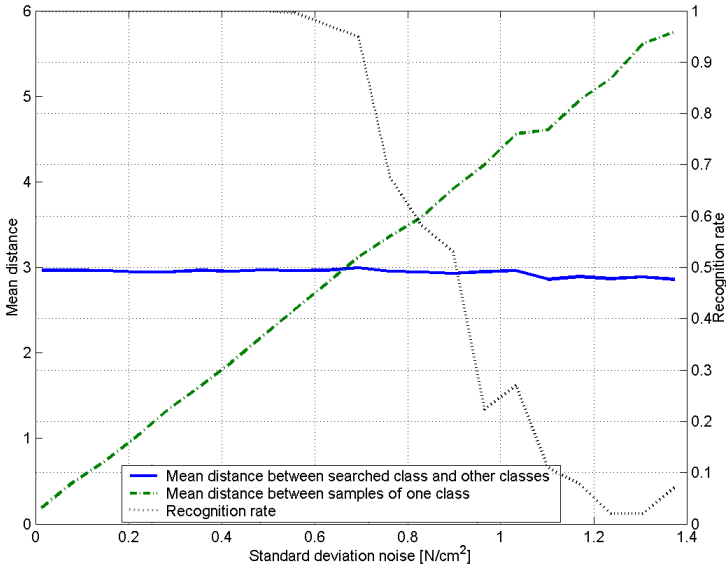


Figure 6.9. Recognition rate and distance between the pressure patterns depending of the standard deviation of the added noise.

The mean of all distances within the same class d_{ms} is almost zero when no additional noise is applied. This distance is caused by the variation of the reference patterns.

The mean of the distances between the classes d_{md} has a value around 3. The variation of d_{md} with respect to the standard deviation of the added noise is below 4% since the mean of the samples within one class stays almost the same. For increasing noise, d_{ms} is linearly increasing from 0.2 at standard deviation 0. For a standard deviation higher than 0.68 N/cm^2 , the value of d_{md} is larger than d_{ms} .

The linear increase of d_{ms} is expected since the noise level is also linearly increasing, causing a linear growing of the size of the sample cloud of a class.

From these results it can be stated that if the noise level can be kept below 10% or $0.5 N/cm^2$, no influence on the classification need be expected.

6.5.1.2. Hysteresis

The scaling factor f_h is altered from 0.1 to 2.0 in steps of 0.1 that corresponds to a d_h of 0.015 to $0.3 N/cm^2$. A value of $f_h = 1.0$ produces hysteresis in same 'size' as in the textile sensor used for the measurements.

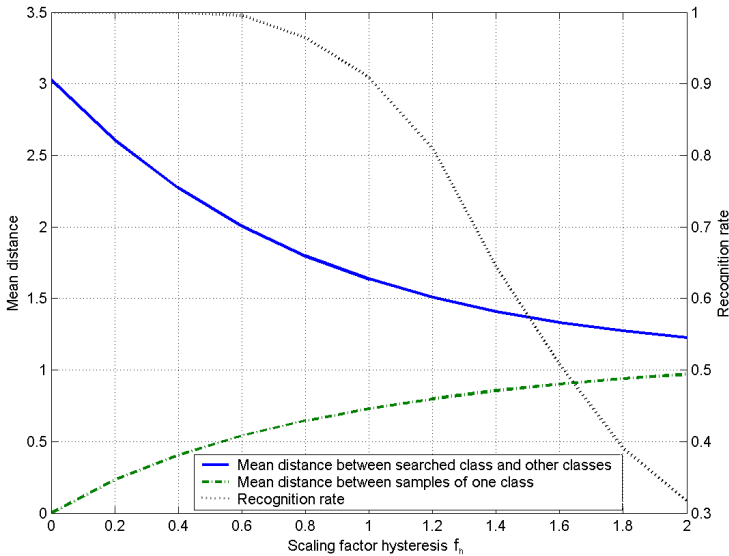


Figure 6.10. Recognition rate and distance between the pressure patterns depending of the 'size' of the hysteresis (scaling factor d_d).

Up to a $f_h = 0.4$ the recognition rate remains unaffected. (fig. 6.10). For increasing hysteresis up to $f_h = 1.2$ the rate drops to 80% and for higher f_h it drops approximately constant to 30% at $f_h = 2.0$. The recognition rate at $f_h = 1$ is around 90%.

The distance between the classes is decreasing for increasing f_h . This behavior is expected since the hysteresis leads to a smaller pressure change between two postures.

The derivation of distance of the samples within a class is decreasing with increasing f_h . This is the origin for the slower decrease of the classification accuracy.

From these results it is expected that compensating the hysteresis in the measured data of the textile sensor will increase the recognition rate by up to 10%. Since the hysteresis can't be exactly modeled and the training data for the classification of the measured data contains also hysteresis, the actual reachable improvement is expected to be less than 10%.

6.5.1.3. Drift

The value of the parameter γ used for modeling the drift (eq. 6.13) is the same as for the textile sensor ($\gamma = -0.025$). The time t is varied from 1 to 1000 seconds in steps of 25 seconds.

The recognition rate decrease is approximately constant for increasing time, but keeps above 90%, also after 1000 s (fig. 6.11).

The distances of the samples within one class keep also small. At $t = 1000$ s the distance is 0.5 what is comparable with a hysteresis with $f_h = 0.5$. The distance between the classes is decreasing for increasing time for the same reason than for the hysteresis; at 1000 s it's value is 2.3.

The change in measured pressure caused by drift is less than 20% from the step size. Noise with a standard deviation of 20% leads to a classification accuracy above 90%. The recognition rate with added hysteresis of factor $f_h = 0.5$ is around 99%. Both recognition rates are in the same region as the recognition rate with drift at 1000 s.

From these results we can expect that drift influences the classification with the data from the textile sensor by less than 10%.

6.5.1.4. Sensor failure

Failing of up to 50 (25%) of 256 sensor elements has no influence on the classification (fig. 6.12). Additional failures lead to a significant decrease of the recognition rate to the minimal rate when all sensor elements fail.

The distance d_{md} between the classes is approximately linearly decreasing for increasing amount of failing sensors. The distance d_{ms} be-

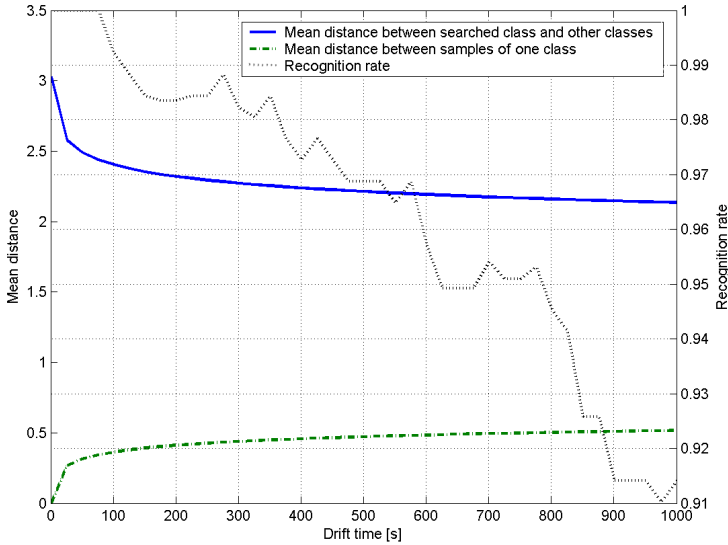


Figure 6.11. Recognition rate and distance between the pressure patterns depending of the drift during time t .

tween the samples of one class is increasing until the half of the sensors fail and is decreasing when more sensors fail.

The reason for this behavior is that a failing sensor element sets the difference between two patterns to zero for this element and therefore the distance between the classes drops. On the other hand, the value of a failing sensor is outside the sample cloud of the corresponding class what leads to an increase of the inner class distance. When all sensors fail, all sensor values are zero and therefore all distances between and also within the classes are zero.

It can be expected that 25% of the 256 sensors can fail without having negative effect. For the textile sensor, the 25% correspond to 24 out of 96 sensors.

6.5.2. Classification from measured patterns

To measure the influence of different error sources, the classification accuracy of the measured data has been determined. The used classifier and features are described in section 6.3.

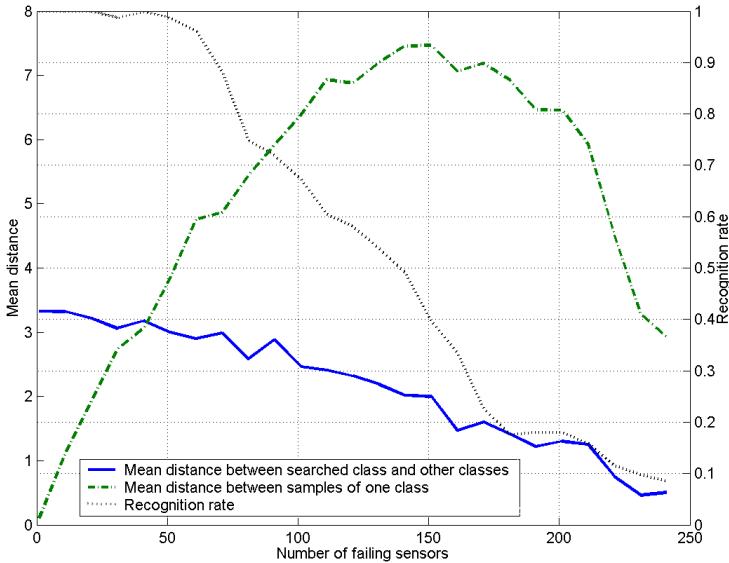


Figure 6.12. Recognition rate and distance between the pressure patterns depending of the number of failing sensors.

The data of 8 subjects have been used as training data and the samples from the remaining subject as test data. The average recognition rate is calculated over all subjects' data used once as test data.

6.5.2.1. Influences from the experiment setup

Besides the discussed error sources in the sections above, other possible influences on the recognition rate have to be investigated. Different positions of the subjects on the chair lead to a translation or rotation of the pressure pattern. Furthermore, a subject can perform the postures slightly differently according to the others. These influences are minimized by giving the subjects precise instructions. The height of the chair has been adopted to the length of the legs and the subjects directed when adopting the positions. Rotation of the body can be excluded by visual inspection during the experiment.

To evaluate the remaining variance of the positioning, the center of force is calculated with the measurements from the reference sys-

tem. The position of the center of force for one subject can be seen in fig 6.13a. The rectangle represents the positions of 90% of the center of forces for all samples for a certain posture. The standard deviation is less than 1 cm for all postures of one subject during all 3 rounds. This is below the resolution of the reference system (1 cm) and textile sensor (5.4 cm). The standard deviations for all subjects are slightly higher but still in most cases less than 2 cm and therefore below the resolution of the textile sensor (fig 6.13b). These values are also below the size of the smallest parts of the buttock (bones). Therefore shifts of the pressure patterns don't lead to a shift to the next sensor element, only to a change in pressure ratio. As a consequence, compensation of translation and rotation is not required.

6.5.2.2. Recognition rate

The recognition rate achieved in [76] is 82% by using 50 sensor elements distributed on the seat and on the back. The same recognition rate has been achieved by optimal placing 19 sensor elements on the chair. A maximal recognition rate of 87% has been reached by using 31 sensors. The data of 52 subjects and 10 postures have been evaluated.

16 postures and 9 subjects have been used in our work. Furthermore, a pressure distribution sensor on the back is not used. Therefore a lower recognition rate as in [76] is expected. The measured distances between the classes with postures conducted once leaning back and once sitting upright (no. 1/5, 6/8, 7/9, 10/12, 11/13) are small (fig. 6.14), what causes confusion between these classes. To obtain better differentiation between these two groups of postures, the textile sensor with one single sensing element has been added as back sensor in our work. This sensor is giving a signal of a pressure of 0.06 N/cm^2 with a standard deviation of 0.07 N/cm^2 for the postures without leaning back and 1.8 N/cm^2 with a standard deviation of 0.34 N/cm^2 for leaning back. It's values are used as additional feature.

When sensor failures and hysteresis are compensated, a recognition rate of 82% with the back sensor and 59% without can be reached with the data from the textile sensor system and the optimal feature set.

The influence on the recognition rate when certain errors are not compensated is shown in the following sections. Without any error compensation, that means using the raw data from the sensor, the recognition rate is 63% with the back sensor and 43% without.

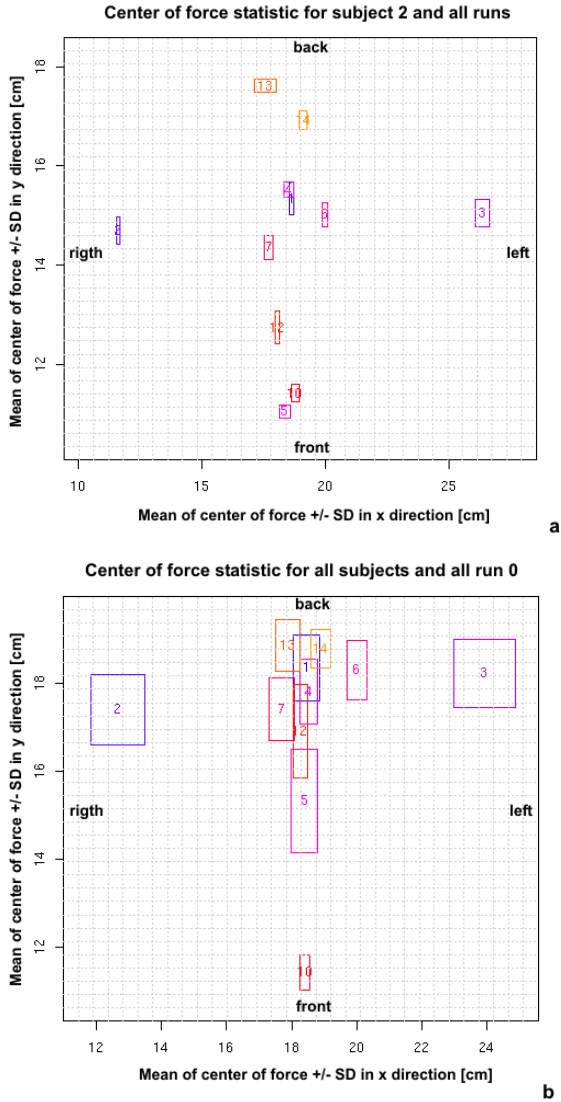


Figure 6.13. Position and standard deviation (rectangles) of the center of force for different postures of one subject in all runs (a) and for all subjects (b).

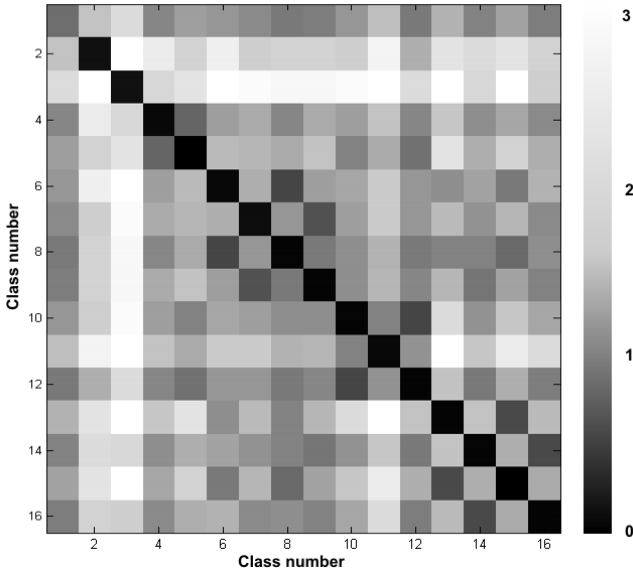


Figure 6.14. Distances between the 16 posture classes for one subject.

6.5.2.3. Hysteresis

To determine the effect of the hysteresis on the classification result, classification was carried out once with the raw data from the textile sensor and once with the data where the hysteresis with the Preisach model introduced in chapter 3 has been compensated.

The average recognition rate for the data with compensated hysteresis is 77% without, and 51% with the back sensor. This is an improvement of 22% and 19% compared to using the raw data.

When the data with compensated failing sensors is used, the enhancement of the recognition rate by modeling the hysteresis is 1% with and 7% without back sensor.

From the simulated data, an improvement of less than 10% of the recognition rate with hysteresis compensation was expected. This fits well with the measured data, when the hysteresis is compensated for the data with compensated failing sensors. The enhancement of the recognition rate compared to using the raw data is higher than the expected 10%. An explanation for this phenomena is, that modeling

the hysteresis reduces also the influence of failing sensors since their pressure values don't drop to zero.

6.5.2.4. Drift

Three runs of measuring all postures have been recorded per subject to determine the influence of drift. The first two runs are one after the other without the subjects standing in between. Before the third run was performed the sensor has been relaxed half an hour without load applied. Drift can be seen between the first and second runs, while drift effects between the first and third runs should be similar.

The data from the first run has been used as training data, the data once from the second and once from the third runs as tests. The difference between the average recognition rate over all subjects is 1% between the two tests. For the data of one particular subject used as test data, the rate differs less than 12% between the two tests.

As a result, it can be stated that influence of the drift is minor on the classification rate compared to the other error sources as expected from the simulation.

6.5.2.5. Sensor failure

The data of some sensor elements of the textile pressure sensor are partially not available due to failing sensors. Shortcuts between the conductive textile parts caused by conductive lint and not ideal connections lead to a malfunction of the corresponding sensor element. Shortcuts or breaks result in capacitance values of zero, so that failing sensor elements can be identified easily.

12 of 96 sensor elements permanently failing leads to a system that has effectively only 84 sensors. Other sensor elements fail irregularly. Some failing is correlated with the postures since the shortcuts can occur when parts are pressed together. The maximum number of sensor elements that fail at least once is 77 during all three rounds for all subjects and 65 for one round. The average is 67 for all three rounds and 58 for one round. Therefore, 57% and 50%, respectively, of the sensor elements are partially failing.

The data of a failing sensor element p_i is replaced by the average value of the four neighboring elements p_l, p_r, p_t, p_b that are available.

$$p_i = \frac{p_l + p_r + p_t + p_b}{n_a} \quad (6.14)$$

with n_a the number of available elements.

If all four are unavailable, the last value available (real or reconstructed) of the sensor element is taken.

The accuracy can be enhanced on average from 43% to 55% without and from 63% to 81% with using the back sensor. This is an improvement of 28% and 29%, respectively. From the results of the simulation (chapter 6.5.1.4), we can expect an enhancement of the recognition between 40% and 50% for 50% of failing sensors. Since the failing of the sensor elements is partially correlated with the postures and therefore contains also information, the measured drop in recognition rate due to failing is less than modeled where the failing is random.

6.6. Conclusion

A comparison of the reached classification accuracies for the different tests can be seen in Table 6.1.

Table 6.1. Recognition rate for data from the textile sensors with different errors compensated.

Data	measured	with back sensor
Raw data	43%	63%
Hysteresis compensated	51%	77%
Failing sensors replaced by mean of adjacent elements	55%	81%
Hysteresis compensated + failing replaced	59%	82%

The classification accuracy reached with the data of the *Tekscan* mat recorded simultaneously is 84% if the data of the textile back sensor is added and the features are optimized for the *Tekscan* data. Without back sensor with the recognition rate drops to 56%.

As a conclusion, it can be stated that the textile sensor performs similarly to the commercial system, if the hysteresis and sensor failures are compensated. Compensating the sensor failure has higher impact on the classification result than modeling the hysteresis.

7

Conclusion

A textile pressure sensor was designed and evaluated. Error sources such as hysteresis and drift have been modeled to compensate for their effect on the measurement. The sensor can be used for the classification of sitting postures when the errors are modeled. It performs similarly to a commercial system.

An outlook provides insight into further improvements and applications of the textile sensor.

7.1. Summary and achievements

Commercial products are available on the market to measure pressure distribution on the human body. These products are not made from textiles and unobtrusive integration into clothing would be a problem.

Therefore, there was a need for a simple textile solution where not only the design is simple but also textile materials could be used off the shelf.

Textile sensors used in research have a rather low accuracy and that prevents them from use as pressure sensing devices [28]. An approach to produce better sensors would be to optimize the materials used and enhance the design of the sensor. In this thesis, we pursue another strategy: Instead of building an exact sensor, the non-idealities and errors are modeled so that they can be compensated for by algorithms.

The major contributions of this thesis are the following:

- A pure textile pressure sensor has been designed and evaluated that can be integrated into clothing to measure pressure distribution on the human body. Using only textiles makes unobtrusive and robust sensors possible. This opens the field for long term operation for medical applications such as supervision of sitting postures, decubitus prevention, muscle activity measurements [75] or control of pressure in medical stockings.
- Models have been evaluated and implemented to quantify hysteresis and drift of the sensor. Only with this modeling is it possible to achieve accurate pressure values from the textile sensor with material that has not been optimized for this application. The errors could be reduced from more than 50% to below 10%. Non ideal and cheaper materials can be used for sensor manufacturing. They don't have to be optimized for linearity and low hysteresis and the system can be less complex. The models also can be easily adopted for other types of pressure sensors and strain sensors.
- The influence of different error sources such as noise, hysteresis, drift and sensor failure has been modeled and analyzed. Their impact has been measured on the classification of sitting postures using pressure patterns.

7.2. Scalability of the system

The geometrical resolution is limited by the minimal size of the sensing elements. To achieve a capacitance greater than 2 pF, the ratio between the area of the electrode and thickness of the spacer has to be greater than 1.9 cm^{-1} . For a spacer of 3 mm thickness this leads to a size of electrodes greater than 6 mm. A spacing of at least 2 mm between adjacent elements is needed when the electrodes are embroidered resulting in a minimal grid distance of 8 mm. This could be reduced if other manufacturing processes such as printing are used. Thinner spacers of $200 \mu\text{m}$ thickness have been used for pressure sensitive retail shelves [73, 74].

The maximal number n of sensors is limited by the sampling frequency f of the measuring system and the desired update rate of the system f_s : $n = f/f_s$. Parallelization increases this number by a factor equal to the number of used parallel systems. In principle there is no limit in sensor quantity as long as the connections can be routed.

The pressure range is defined by the used spacer and is only limited by the availability of appropriate spacers.

7.3. Conclusions

The following conclusions can be drawn from the results of the thesis:

- The sensing quality of the textile sensor can be significantly improved by modeling the behavior of the sensor. The error can be reduced from more than 50% to below 10%. The used models are also valid for other types of pressure or even strain sensors; modification of the parameters are needed.
- It is possible to use standard textiles for pressure sensing.
- Even with this solution, special investigation had to be made when selecting the material. Several types of conductive yarn are available on the market. Nevertheless, it has become evident that it is difficult to find an appropriate yarn for the textile sensor with multiple sensing elements. The yarn we finally used appeared to be not perfect but usable for applications where failure of certain sensors can be tolerated. For other applications, such as for medical use, this problem has to be solved. Besides this, the goal of using standard material has been reached. Single sensors manufactured with different yarn and conductive garment instead of

embroidered electrodes were shown as reliable after years of regular use.

- The textile sensor has proven its usefulness as a sensing device for the classification of sitting postures with a recognition rate of 61% when sensor failures and hysteresis are compensated. This value is higher than the classification rate of 48% by using a commercial pressure sensing mat from Tekscan.

7.4. Outlook

The sensor principle proved it works. The specifications stated at the beginning of this thesis are fulfilled. Nevertheless the sensor can be improved further in different areas.

7.4.1. Material and technology

Improvements in measuring technologies for small capacitances can enhance the sampling rate of the sensor. This makes it possible to measure larger arrays with a reasonable speed without the need of parallel measuring. The size of the electronics can be reduced if the switching circuit or even the whole sensing part is integrated into an FPGA or other appropriate device.

Robustness of the sensor can be improved further. The conductive yarn has been shown as the bottleneck, while other components are as robust as normal textiles. Better yarn has to be developed that doesn't cause shortcuts but is still usable in embroidering machines and robust enough. Yarns with fibres twined around a textile carrier are best for ensuring few shortcuts. However, the production of such a yarn isn't stable enough to obtain a yarn that can be processed without causing problems in the machines; its conductivity has to remain in the specified range even after hundreds time of washing. Using the sensor in medical environment demands highest reliability, not yet given with the 240 elements prototype but reachable with suitable yarn.

Laminating the conductive parts after the embroidering process could further reduce the risk of shortcuts. However the textiles get stiff and lose their textile properties. A laminating process has to be found without this drawback. Using insulated yarn is another possibility. Removing the coating for getting electrical contact between the yarns has been shown as complicated. Manual removal is time consuming and thermal processes destroy the carrying yarn and that should be

prevented. Lasers could be used for automatic removal of the coating [59]. All these methods are not applicable to multi filament yarn where the polyester is coated with conductive material. This material would also be removed with the coating. Only a chemical solution would be applicable.

7.4.2. Production and commercialization

To turn the sensor from a research prototype into a commercial product, several aspects have to be evaluated:

- Methods have to be found for fast manufacturing at low effort. The prototypes need a large amount of manual assembling. Two weeks are needed per sensor for sewing the embroidered electrodes together with the connections, removing shortcuts and for testing. Methods or machines have to be developed especially for automatic connecting the electrodes with the connection lines.
- The use of the sensor in clothing or directly on the body will have to be made in accordance with various regulations. These aspects have not been investigated so far.

7.4.3. Further use and applications

We intend to investigate the commercialization of the textile sensor in a following CTI¹ project where a sensing mat will be constructed for measuring the pressure distribution in a bed to prevent decubitus.

In the SEAT project [7], a pressure sensing mat will be integrated into an airplane seat as an additional sensor for evaluating the comfort and state of a passenger. The classification of sitting postures can be used as basis for detecting the users action and constitution.

¹The CTI is the Swiss Confederation's innovation promotion agency

A

APPENDIX A

A.1. Error measures

A.1.1. Nomenclature

x_m measured value
 x_t true value

A.1.2. Absolute error

$$e_a = x_m - x_t \quad (\text{A.1})$$

A.1.3. Relative error

$$e_r = \frac{x_m - x_t}{x_t} = \frac{e_a}{x_t} \quad (\text{A.2})$$

Average relative error

$$e_{r, av} = \frac{1}{n} \sum_{k=1}^n e_r \quad (\text{A.3})$$

A.1.4. Offset

$$e_o = x_m \text{ for } x_t = 0 \quad (\text{A.4})$$

A.1.5. Linearity error of AD/DA converters

- The **integral** linearity error is the maximum deviation of the transfer characteristic of a converter from a straight line.
- The **differential** linearity error of a converter is defined as the relative error in analog signal when a change of 1 lsb occurs.

Glossary

Symbols

Name	SI Unit	Meaning	Introduced
α		parameter of relay operator	4.3.1
β		parameter of relay operator	4.3.1
ϵ	$C^2N^{-1}m^{-2}$	permittivity	2.3.2
γ		scaling factor drift	5.2
ω_0	s^{-1}	oscillation frequency	3.2.1.1
τ	s	time constant	3.2.2.1
A	m^2	area	2.3.2
c		class	6.4.2
C	F	capacitance	2.3.2
C_x	F	capacitance of a sensor element	3.2.1.1
C_p	F	parasitic capacitance	3.2.1.1
C_{ref}	F	reference capacitance	3.2.1.4
d	m	distance between the electrodes	2.3.2
d_c		distance between classes	6.4.2
d_{md}		mean of distances between classes	6.4.2
d_{md}		mean of distances of samples within one class	6.4.2
d_s	m	spacing electrodes	2.3.2.2
d_l	m	spacing connection lines	2.3.2.2
dt	s	time step	
e_r		relative error	A
e_a		absolute error	A
F	N	force	
f	s^{-1}	frequency	
f_h		scaling factor hysteresis	6.4.4

$h(t)$		hysteresis model output	4.3.1
I	A	current	
k	$J \cdot K^{-1}$	Boltzmann constant	3.2.1.1
M		local maxima of input hysteresis model	4.4
m		local minima of input hysteresis model	4.4
n_e		number of electrodes	2.3.2.1
n_s		number of stripes	2.3.2.1
n_c		number of connections	2.3.2.1
n_l		number of connection lines	2.3.2.2
p	N/m^2	pressure	
$p_{i,t}$	N/m^2	pressure on element i of pattern t	6.4.4
PN_{min}		minimal phase noise	3.2.1.1
R	Ω	resistance	
s	N/m^2	size of pressure step	5.1.2.1
t	s	time	
T	K	temperature	3.2.1.1
V	V	voltage	
V_{src}	V	source voltage	3.2.1.1
V_{ref}	V	reference voltage	3.2.3.3
Z	Ω	impedance	3.2.1.3

Acronyms and Abbreviations

ADC	analog to digital converter
DAC	digital to analog converter
FPGA	field programmable gate array
IC	integrated circuit
opamp	operation amplifier
PCB	printed circuit board
PLL	phase locked loop
PU	polyurethane
PE	polyethylene
SD	standard deviation

Bibliography

- [1] 24-bit capacitance-to-digital converter with temperature sensor, analog devices, 2005. 37
- [2] The inductance and capacitance meter projects, 2005. URL <http://braincambre500.freeservers.com/indcap.htm>. 31
- [3] Permittivität - wikipedia, the free encyclopedia, 2007. URL <http://de.wikipedia.org/wiki/Permittivitaet>. 42
- [4] Permittivity - wikipedia, the free encyclopedia, 2007. URL <http://en.wikipedia.org/wiki/Permittivity>. 42
- [5] Compression stockings - wikipedia, the free encyclopedia, 2008. URL http://en.wikipedia.org/wiki/Compression_stockings. 11
- [6] Kelvin (4-wire) resistance measurement, 2008. URL http://www.allaboutcircuits.com/vol_1/chpt_8/9.html. 11
- [7] Seat project, 2008. URL <http://www.seat-project.org/>. 4, 101
- [8] Smart products need smart solutions - universal transducer interface - revolution in sensor interfacing, smartec by, June 1995. 36
- [9] H. Brem and C. Lyder. Protocol for the successful treatment of pressure ulcers. *Am J Surg*, pp. 9–17, 2004. 3
- [10] P. H. af Segerstad, R. Larsson, and S. Toll. Micro-mechanical model of a viscoplastic open cell foam. In *International Conference on Computational Plasticity*, 2005. 52
- [11] O. Amft, H. Junker, P. Lukowicz, G. Troster, and C. Schuster. Sensing muscle activities with body-worn sensors. *Wearable and Implantable Body Sensor Networks, 2006. BSN 2006. International Workshop on*, pp. 138–141, April 2006. 2, 11
- [12] C. Ashruf. Thin flexible pressure sensors. *Sensor Review*, 22(4): 322–327, 2002. 2, 11

- [13] M. Avalle, G. Belingardi, and A. Ibba. Mechanical models of cellular solids: Parameters identification from experimental tests. *International Journal of Impact Engineering*, 34(1):3–27, January 2007. 52
- [14] T. Azeroth. *Aufbau eines textilen Drucksensors zur dreidimensionalen Visualisierung der Druckverteilung*. Praxisarbeit, ITP GmbH, 2005. 3
- [15] B. Barrois, F. A. Allaert, and D. Colin. A survey of pressure sore prevalence in hospitals in the greater paris region. *J Wound Care*, pp. 234–6, 1995. 3
- [16] P. Binkley. Predicting the potential of wearable technology. *Engineering in Medicine and Biology Magazine, IEEE*, 22(3):23–27, May-June 2003. 2
- [17] R. Bouc. Forced vibrations of a mechanical system with hysteresis. In *Proceedings of the 4th Conference on Nonlinear Oscillations*, 1967. 52
- [18] G. H. Brandeis, J. N. Morris, D. J. Nash, and L. A. Lipsitz. The epidemiology and natural history of pressure ulcers in elderly nursing home residents. *Jama*, pp. 2905–9, 1990. 3
- [19] J. Chen, Z. Fan, J. Engel, and C. Liu. Towards modular integrated sensors: the development of artificial haircell sensors using efficient fabrication methods. *Intelligent Robots and Systems, 2003. (IROS 2003). Proceedings. 2003 IEEE/RSJ International Conference on*, 3:2341–2346 vol.3, Oct. 2003. 2
- [20] M.-Y. Cheng, W.-Y. Chang, L.-C. Tsao, S.-A. Yang, Y.-J. Yang, W.-P. Shih, F.-Y. Chang, S.-H. Chang, and K.-C. Fan. Design and fabrication of an artificial skin using pi-copper films. *Micro Electro Mechanical Systems, 2007. MEMS. IEEE 20th International Conference on*, pp. 389–392, Jan. 2007. 2
- [21] L. Chua and S. Bass. A generalized hysteresis model. *Circuits Theory, IEEE Transactions on [legacy, pre - 1988]*, 19(1):36–48, Jan 1972. 52
- [22] D. De Rossi, A. Nannini, and C. Domenici. Artificial sensing skin mimicking mechanolectrical conversion properties of human

- dermis. *Biomedical Engineering, IEEE Transactions on*, 35(2): 83–92, Feb 1988. 2
- [23] T. Dillard. 3d quantitative image analysis of open-cell nickel foams under tension and compression loading using x-ray microtomography. *Philosophical Magazine*, 85:2147–2175(29), 1 July 2005. 51
- [24] J. v. Drecht. Relaxatie oscillator, 1991. Pat. Appl. 91.01076. 34
- [25] A. Ducker. Pressure ulcers: assessment, prevention, and compliance. *Case Manager*, 13(4):61–4, Jul-Aug 2002. 3
- [26] R. O. Duda, P. Hart, and D. Stork. *Pattern Classification (2nd Edition)*. Wiley-Interscience, 2000. 77, 81
- [27] L. Dunne, S. Brady, B. Smyth, and D. Diamond. Initial development and testing of a novel foam-based pressure sensor for wearable sensing. *J NeuroEngineering Rehabil*, 2(4), 2005. 2
- [28] L. Dunne, R. Tynan, G. O’Hare, B. Smyth, S. Brady, and D. Diamond. Coarse sensing of upper arm position using body-garment interactions. In *Proc. of the 2nd International Forum on Applied Wearable Computing*, pp. 138–141, 2005. 2, 11, 98
- [29] U. Ehrenberg. *Entwurf eines selbstabgleichenden kapazitiven Sensors zur Grenzstandserfassung von Flüssigkeiten*. Diploma thesis, Technische Universität Ilmenau, 2000. 26, 28, 31, 32
- [30] Endress and H. Ltd. A capacitance comparator measuring circuit, 1984. UK Patent 84087. 32
- [31] J. Engel, J. Chen, X. Wang, Z. Fan, C. Liu, and D. Jones. Technology development of integrated multi-modal and flexible tactile skin for robotics applications. *Intelligent Robots and Systems, 2003. (IROS 2003). Proceedings. 2003 IEEE/RSJ International Conference on*, 3:2359–2364 vol.3, Oct. 2003. 2
- [32] D. H. Everett and W. I. Whitton. A general approach to hysteresis. *Transactions of the Faraday Society*, 48:749–757, 1952. 53
- [33] M. A. Fergenbaum, H. Lindsay, J. M. Stevenson, E. Morin, and J. Bryant. Pressure measurement applications for humans. Technical report. 4

- [34] M. A. Fergenbaum, J. M. Stevenson, E. Morin, J. Bryant, L. Haddock, and S. A. Reid. Assessment of pressure measurement systems on flat surfaces. In *Annual Meeting American Society of Biomechanics*, 2003. 4
- [35] W. J. Fuller Brown. Failure of the local-field concept for hysteresis calculations. *Journal of Applied Physics*, 33:1308–1309, Mar. 1962. 53
- [36] U. Ganguly. Rc-oscillator synthesis: Sub-audio-frequency generation with a single control. *Proceedings of the IEEE*, 66(4): 516–518, April 1978. 25
- [37] L. J. Gibson and M. F. Ashby. *Cellular Solid Structure and Properties*. Cambridge University Press, 1997. 52
- [38] F. v. d. Goes. *Lost-cost smart sensor interfacing*. Ph.d. thesis, Delft University of Technology, 1996. 35
- [39] C. Gokcek. Tracking the resonance frequency of a series rlc circuit using a phase locked loop. *Control Applications, 2003. CCA 2003. Proceedings of 2003 IEEE Conference on*, 1:609–613 vol.1, 23-25 June 2003. 27
- [40] R. B. Gorbet. *Control of hysteretic systems with preisach representations*. Ph.d. thesis, University of Waterloo, Waterloo, Canada, 1997. 55
- [41] J. Grzyb, I. Ruiz, D. Cottet, and G. Troster. An investigation of the material and process parameters for thin-film mcm-d and mcm-l technologies up to 100ghz. *Electronic Components and Technology Conference, 2003. Proceedings. 53rd*, pp. 478–486, May 27-30, 2003. 42
- [42] T. Harada, T. Mori, Y. Nishida, T. Yoshimi, and T. Sato. Body parts positions and posture estimation system based on pressure distribution image. *Robotics and Automation, 1999. Proceedings. 1999 IEEE International Conference on*, 2:968–975 vol.2, 1999. 4
- [43] P. Harrop. *Dielectrics*. Wiley, New York, 1972. 26
- [44] A. Holt and M. Lee. A class of rc oscillators. *Proceedings of the IEEE*, 55(6):1119–1119, June 1967. 25

- [45] S. M. Huang, A. L. Stott, R. G. Green, and M. S. Beck. Electronic transducers for industrial measurement of low value capacitances. *Journal of Physics E: Scientific Instruments*, 21(3):242–250, 1988. 26, 29, 32, 41
- [46] B. A. Ichijo. On the method of measuring dielectric constant and loss angles of semiconductors. *J. Appl. Phys.*, 23:307–11, 2003. 27
- [47] A. Imad, A. Ouâkka, K. D. Van, and G. Mesmacque. Analysis of the viscoelastoplastic behavior of expanded polystyrene under compressive loading: Experiments and modeling. *Strength of Materials*, 33(2):140–9, March 2001. 62
- [48] A. Jayasuriya, S. Tasaka, and N. Inagaki. Pyroelectric properties of linear aromatic polyurethanes. *Dielectrics and Electrical Insulation, IEEE Transactions on*, 3(6):765–769, Dec 1996. 42
- [49] R. Kageyama, S. Kagami, M. Inaba, and H. Inoue. Development of soft and distributed tactile sensors and the application to a humanoid robot. *Systems, Man, and Cybernetics, 1999. IEEE SMC '99 Conference Proceedings. 1999 IEEE International Conference on*, 2:981–986 vol.2, 1999. 2
- [50] O. Kerpa, K. Weiss, and H. Worn. Development of a flexible tactile sensor system for a humanoid robot. *Intelligent Robots and Systems, 2003. (IROS 2003). Proceedings. 2003 IEEE/RSJ International Conference on*, 1:1–6 vol.1, Oct. 2003. 2
- [51] C. Kirchmair. Ein Gradientenabstiegsverfahren zum schätzen der Parameter des Preisach Modells für Hysterese, 1999. Institut für Informatik, Technische Universität München. 56
- [52] J. Kittler. Feature set search algorithms. *Pattern Recognition and Signal Processing*, pp. 41–60, 1978. 79
- [53] M. Klann. Playing with fire: Participatory design of wearable computing for fire fighters. In *Conference on Human Factors in Computing Systems*, April 28 - Mai 3 2007. 2
- [54] M. A. Krasnosel'skii and A. V. Pokrovskii. *Systems with Hysteresis*. Springer-Verlag, 1989. 52

- [55] J. S. Krause and L. Broderick. Patterns of recurrent pressure ulcers after spinal cord injury: identification of risk and protective factors 5 or more years after onset. *Arch Phys Med Rehabil*, 85: 1257–6, 2004. [3](#)
- [56] G. Krishna and K. Rajanna. Tactile sensor based on piezoelectric resonance. *Sensors, 2002. Proceedings of IEEE*, 2:1643–1647 vol.2, 2002. [11](#)
- [57] J. Kung, R. Mills, and H.-S. Lee. Digital cancellation of noise and offset for capacitive sensors. *Instrumentation and Measurement, IEEE Transactions on*, 42(5):939–942, Oct 1993. [33](#), [34](#)
- [58] E. Landis. Microinjections studies of capillary blood pressure in human skin. *Heart*, (15):209 – 228, 1930. [3](#)
- [59] I. Locher, T. Kirstein, and G. Tröster. Routing methods adapted to e-textiles. In *Proc. 37th International Symposium on Microelectronics (IMAPS 2004)*, November 2004. [101](#)
- [60] I. Locher, T. Kirstein, and G. Tröster. Temperature profile estimation with smart textiles. In *Proc. 1st International Scientific Conference Ambience 05*, September 2005. [2](#)
- [61] I. Locher, M. Klemm, T. Kirstein, and G. Trster. Design and characterization of purely textile patch antennas. *Advanced Packaging, IEEE Transactions on*, 29(4):777–788, Nov. 2006. [2](#), [42](#)
- [62] P. Lukowicz, F. Hanser, C. Szubski, and W. Schobersberger. Detecting and interpreting muscle activity with wearable force sensors. In K. P. Fishkin, B. Schiele, P. Nixon, and A. J. Quigley, ed., *Pervasive*, vol. 3968 of *Lecture Notes in Computer Science*, pp. 101–116. Springer, 2006. [2](#), [11](#)
- [63] V. Lumelsky, M. Shur, and S. Wagner. Sensitive skin. *Sensors Journal, IEEE*, 1(1):41–51, Jun 2001. [2](#)
- [64] C. Lyder, C. Yu, D. Stevenson, R. Mangat, O. Empleo-Frazier, J. Emerling, and J. McKay. Validating the braden scale for the prediction of pressure ulcer risk in blacks and latino/hispanic elders: a pilot study. *Ostomy Wound Manage*, 44:42–49, 1998. [3](#)
- [65] C. H. Lyder. Pressure ulcer prevention and management. *Jama*, 289:223–6, 2003. [3](#)

- [66] P. Mahalanobis. On the generalised distance in statistics. vol. 12, pp. 49–55. the National Institute of Sciences of India, 1936. 81
- [67] K. Martin. A voltage-controlled switched-capacitor relaxation oscillator. *Solid-State Circuits, IEEE Journal of*, 16(4):412–414, Aug 1981. 34
- [68] C. Mattmann, T. Kirstein, and G. Tröster. A method to measure elongations of clothing. In *Proc. 1st International Scientific Conference Ambience 05*, September 2005. 2
- [69] C. Mattmann and G. Tröster. Design concept of clothing recognizing back postures. In *Proc. 3rd IEEE-EMBS International Summer School and Symposium on Medical Devices and Biosensors (ISSS-MDBS 2006)*, September 2006. 2
- [70] I. Maurtua, P. T. Kirisci, T. Stiefmeier, M. L. Sbodio, and H. Witt. A wearable computing prototype for supporting training activities in automative production. In *4th International Forum on Applied Wearable Computing (IFAWC)*, March 12 - 13, 2007. 2
- [71] I. Mayergoyz and G. Friedman. Generalized preisach model of hysteresis. *Magnetics, IEEE Transactions on*, 24(1):212–217, Jan 1988. 54
- [72] G. Meijer, J. van Drecht, P. de Jong, and H. Neuteboom. New concepts for smart signal processors and their application to psd displacement transducers. *Sensors and Actuators A*, 35:23–30, 1992. 36
- [73] C. Metzger, E. Fleisch, J. Meyer, M. Dansachmüller, I. Graz, M. Kaltenbrunner, C. Keplinger, R. Schwödauauer, and S. Bauer. Flexible-foam-based capacitive sensor arrays for object detection at low cost. *Applied Physics Letters*, 92(1):013506–+, Jan. 2008. 99
- [74] C. Metzger, J. Meyer, E. Fleisch, and G. Tröster. Weight-sensitive foam to monitor product availability on retail shelves. In *Pervasive*, vol. 4480 of *Lecture Notes in Computer Science*, pp. 268–279. Springer, 2007. 99

- [75] J. Meyer, P. Lukowicz, and G. Tröster. Textile pressure sensor for muscle activity and motion detection. In *10th IEEE International Symposium on Wearable Computers*, pp. 69–72, 2006. **10, 98**
- [76] B. Mutlu, A. Krause, J. Forlizzi, C. Guestrin, and J. Hodgins. Robust, low-cost, non-intrusive sensing and recognition of seated postures. In *UIST '07: Proceedings of the 20th annual ACM symposium on User interface software and technology*, pp. 149–158, New York, NY, USA, 2007. ACM. **3, 74, 91**
- [77] R. Nadal-Guardia, A. Brosa, and A. Dehe. Ac transfer function of electrostatic capacitive sensors based on the 1-d equivalent model: application to silicon microphones. *Microelectromechanical Systems, Journal of*, 12(6):972–978, Dec. 2003. **32**
- [78] R. Nadal-Guardia, A. Brosa, and A. Dehe. Constant charge operation of capacitor sensors based on switched-current circuits. *Sensors Journal, IEEE*, 3(6):835–842, Dec. 2003. **33**
- [79] R. Navid, T. Lee, and R. Dutton. Minimum achievable phase noise of rc oscillators. *Solid-State Circuits, IEEE Journal of*, 40(3):630–637, March 2005. **25**
- [80] G. Novak. The femto capacitance meter, 2006. URL <http://nov55.com/cap/cap1.htm>. **32, 38**
- [81] C. Nørstebø. Intelligent textiles, soft products. Technical report, 2003. **4**
- [82] T. V. Pernegerab, A.-C. Raëc, J.-M. Gaspoz, F. Borste, O. Vitek, and C. Hélotc. Screening for pressure ulcer risk in an acute care hospital: development of a brief bedside scale. *J Clin Epidemiol*, 55:498–504, 2002. **3**
- [83] D. B. Poyen. *Stiffness, Damping and Creep Properties of a Polyurethane Foam Including the Effects of Temperature and Humidity*. Her Majesty’s Stationery Office, 1967. **63**
- [84] F. Preisach. Über die magnetische Nachwirkung. *Zeitschrift für Physik*, 94:277–302, 1935. **53**
- [85] F. Reverter, X. Li, and G. C. M. Meijer. A novel interface circuit for grounded capacitive sensors with feedforward-based active shielding. *Measurement Science and Technology*, 19(2):025202 (5pp), 2008. **41**

- [86] K. Richter and M. Möbius. Sensoric textile bed cover. *MST News*, pp. 35–6, 2005. 3
- [87] A. Riener and A. Ferscha. Driver activity recognition from sitting postures. In *Mensch und Computer 2007, Workshop Automotive User Interfaces, Weimar, Germany*, pp. 55–63. Verlag der Bauhaus-Universität Weimar, September 2007. 4
- [88] A. Riener and A. Ferscha. Supporting implicit human-to-vehicle interaction: Driver identification from sitting postures. In *The First Annual International Symposium on Vehicular Computing Systems (ISVCS 2008)*, Trinity College Dublin, Ireland, July 2008. ACM Digital Library. 4
- [89] P. Sain, M. Sain, and B. Spencer. Models for hysteresis and application to structural control. *American Control Conference, 1997. Proceedings of the 1997*, 1:16–20, Jun 1997. 52, 53
- [90] M. Sanduleanu and J. Frambach. 1ghz tuning range, low phase noise, lc oscillator with replica biasing common-mode control and quadrature outputs. *Solid-State Circuits Conference, 2001. ESS-CIRC 2001. Proceedings of the 27th European*, pp. 506–509, 18-20 Sept. 2001. 25
- [91] M. Sasani and E. P. Popov. Seismic energy dissipators for rc panels: Analytical studies. *Journal of Engineering Mechanics ASCE*, 127:835–843, 2001. 52
- [92] F. Scarpa and F. C. Smith. Passive and mr fluid-coated auxetic pu foam - mechanical, acoustic, and electromagnetic properties. *J of Intelligent Material Systems and Structures*, 15(12):973–9, 2004. 42
- [93] L. W. Schwartz and R. V. Roy. A mathematical model for an expanding foam. *Journal of Colloid and Interface Science*, 264 (1):237–249, August 2003. 52
- [94] M. Sergio, N. Manaresi, F. Campi, R. Canegallo, M. Tartagni, and R. Guerrieri. A dynamically reconfigurable monolithic cmos pressure sensor for smart fabric. *Solid-State Circuits, IEEE Journal of*, 38(6):966–975, June 2003. 2

- [95] M. Sergio, N. Manaresi, M. Tartagni, R. Guerrieri, and R. Cane-gallo. A textile based capacitive pressure sensor. *Sensors, 2002. Proceedings of IEEE*, 2:1625–1630 vol.2, 2002. 28
- [96] M. Shimojo, A. Namiki, M. Ishikawa, R. Makino, and K. Mabuchi. A tactile sensor sheet using pressure conductive rubber with electrical-wires stitched method. *Sensors Journal, IEEE*, 4(5):589–596, Oct. 2004. 2
- [97] L. A. Slivovsky. *A real-time sitting posture tracking system*. Phd thesis, Purdue University, 2001. 3
- [98] L. A. Slivovsky and H. Z. Tan. A real-time sitting posture tracking system. In *Proceedings of the Ninth (9th) International Symposium on Haptic Interfaces for Virtual Environment and Teleoperator Systems*, vol. 69, pp. 1049–1056. American Society of Mechanical Engineers Dynamic Systems and Control Division, 2000. 3
- [99] P. Srinivasan, D. Birchfield, G. Qian, and A. Kidané. A pressure sensing floor for interactive media applications. In *ACE '05: Proceedings of the 2005 ACM SIGCHI International Conference on Advances in computer entertainment technology*, pp. 278–281, New York, NY, USA, 2005. ACM. 4
- [100] M. Stäger, H. Junker, M. von Waldkirch, and G. Tröster. Using wearables in maintenance: A modular test platform. In *TCMC 2003: Workshop on Wearable Computing*, Mar. 2003. 2
- [101] R. Stevens, B.; Manning. Improvements in the theory and design of rc oscillators. *Circuits and Systems, IEEE Transactions on*, 18(6):636 – 643, 1988. 25
- [102] T. Stiefmeier, D. Roggen, G. Tröster, G. Ogris, and P. Lukowicz. Wearable activity tracking in car manufacturing. *Pervasive Computing, IEEE*, 7(2):42–50, April-June 2008. 2
- [103] J. M. Sullivan. The geometry of bubbles and foams. *Foams and emulsions*, 354:379–402, 1999. 52
- [104] B. Suthar, D. Klempner, K. C. Frisch, Z. Petrovic, and Z. Jelcic. Novel dielectrics from ipns derived from castor oil based polyurethanes. *Journal of Applied Polymer Science*, 53(8):1083–1090, 1994. 42

- [105] T. Sych. *Estimation of geometric characteristics of foam structures*. Diploma thesis, Technical University Kaiserslautern, 2004. [52](#)
- [106] R. Tajima. Development of soft and distributed tactile sensors and the application to a humanoid robot. *Advanced Robotics*, 16: 381–397(17), 1 July 2002. [2](#)
- [107] H. Tan, L. Slivovsky, and A. Pentland. A sensing chair using pressure distribution sensors. *Mechatronics, IEEE/ASME Transactions on*, 6(3):261–268, Sep 2001. [3](#)
- [108] J. Tapson and J. Greene. Improved capacitance measurement by means of resonance locking. *Measurement Science and Technology*, 5:20–26(7), 1994. [26](#)
- [109] F. Toth, G. Meijer, and H. Kerkvliet. Ultra-linear, low-cost measurement system for multi-electrode pf-range capacitors. *Instrumentation and Measurement Technology Conference, 1995. IMTC/95. Proceedings. 'Integrating Intelligent Instrumentation and Control'*, IEEE, pp. 512–, Apr 1995. [35](#)
- [110] F. N. Toth. *EA design methodology for low-cost, high-performance capacitive sensors*. Ph.d. thesis, Delft University of Technology, 1997. [12](#), [26](#), [33](#), [34](#), [36](#), [40](#)
- [111] A. Tschürtz and A. Andjic. *Entwicklung einer elektrischen Schaltung zur Auswertung kleiner Kapazitätsänderungen*. Semester thesis, Aalen University, 2003. [26](#)
- [112] F. Van Der Goes and G. Meijer. A novel low-cost capacitive-sensor interface. *Instrumentation and Measurement, IEEE Transactions on*, 45(2):536–540, Apr 1996. [35](#)
- [113] J. van Drecht, G. Meijer, and P. de Jong. Concepts for the design of smart sensors and smart signal processors and their application to psd displacement transducers. *Solid-State Sensors and Actuators, 1991. Digest of Technical Papers, TRANSDUCERS '91., 1991 International Conference on*, pp. 475–478, Jun 1991. [36](#)
- [114] J. Walter, J. Sacks, R. Othman, A. Rankin, B. Nemchausky, R. Chintam, and J. Wheeler. A database of self-reported secondary medical problems among va spinal cord injury patients:

- its role in clinical care and management. *J Rehabil Res Dev*, 39 (1):53–61, Jan-Feb 2002. **3**
- [115] Y. K. Wen. Method of random vibration of hysteretic systems. *Journal of Engineering Mechanics ASCE*, 102:249–263, 1976. **52**
- [116] R. Wijesiriwardana, K. Mitcham, and T. Dias. Fibre-meshed transducers based real time wearable physiological information monitoring system. *Wearable Computers, 2004. ISWC 2004. Eighth International Symposium on*, 1:40–47, Oct.-3 Nov. 2004. **11**
- [117] R. Wojtyna and A. Borys. Contribution to the linear theory of frequency stability of rc oscillators. *Circuits and Systems, IEEE Transactions on*, 33(4):418–424, Apr 1986. **25**
- [118] J. G. Woodward and E. Della Torre. Particle interaction in magnetic recording tapes. *Journal of Applied Physics*, 31:398–+, Feb. 1960. **53**
- [119] W. Yang, M. Brant, and M. Beck. A multi-interface level measurement system using a segmented capacitance sensor for oil separators. *Measurement Science and Technology*, 5:1177–1180(4), 1994. **29**

Curriculum Vitae

Personal Information

Jan Meyer

Born 28 March 1978, Berne BE, Switzerland

Citizen of Muri BE, Switzerland

Education

- 2003–2008 PhD studies in information technology and electrical engineering (Dr. sc. techn.) at ETH Zurich, Switzerland
- 1998–2003 MSc studies in information technology and electrical engineering (Dipl. El.-Ing. ETH) at ETH Zurich, Switzerland
- 1993–1998 Gymnasium (Matura, Typus C) at Gymnasium Bern-Kirchenfeld, Berne, Switzerland
- 1985–1993 Primary and Secondary school in Berne, Switzerland

Professional Experience

- 2003–2008 Research and teaching assistant at Electronics Laboratory, ETH Zurich, Switzerland
- 2000, 2001 Internship with Siemens Landis+Stäfa, Stäfa, Switzerland
- 1999 Internship with Ascom, Bern, Switzerland
Course on Basic engineering skills